Computers and Chemical Engineering 172 (2023) 108173

Contents lists available at ScienceDirect

Computers and Chemical Engineering

journal homepage: www.elsevier.com/locate/cace

Online detrended fluctuation analysis and improved empirical wavelet transform for real-time oscillations detection in industrial control loops

Wahiba Bounoua [a,*], Muhammad Faisal Aftab [a], Christian Walter Peter Omlin [b]

[a] Department of Engineering Sciences, University of Agder, 4879 Grimstad, Norway
[b] Center for Artificial Intelligence Research, University of Agder, 4879 Grimstad, Norway

ARTICLE INFO

Keywords:
Controller performance monitoring
Detrended fluctuation analysis
Improved empirical wavelet transform
Oscillations detection and characterisation

ABSTRACT

Detrended Fluctuation Analysis (DFA) is a reliable and assumption-free approach for gauging the complexity of a time series. In this paper, an online oscillations detection paradigm is presented, which integrates the potential of DFA in detecting abnormal coherent fluctuations with the Empirical Wavelet Transform (EWT) efficiency in extracting the characteristics of oscillations. However, the standard EWT fails to separate modes oscillating at close frequencies, resulting in an incorrect decomposition. Furthermore, the lack of an appropriate stopping criterion frequently results in the signal being over-decomposed into several inconsequential components. Therefore, owing to the capability of DFA to differentiate between fluctuations stemming from noise and coherent fluctuations arising from genuine oscillations, an Improved EWT (IEWT) is presented to mitigate these issues and accurately extract only compelling oscillating modes. The proposed DFA-based IEWT framework is verified on simulated applications and data from real industrial processes, illustrating its effectiveness.

1. Introduction

In the field of safety–critical industries, such as chemical, construction, metals, and mining, real-time monitoring is a challenging task that researchers are still striving to achieve. The objective is to promptly detect faults before they evolve into failures that seriously endanger human health and the environment (National Research Council, 1997; Chau et al., 2022; Amin and Khan, 2022). The industrial incidents – occurring as a result of improper monitoring – have been constantly investigated through organisations like the Chemical Safety Board (CSB) (CSB, n.d.) and Health and Safety Executive (HSE) (HSE, n.d.). Correspondingly, they emphasise the importance of adequate monitoring and delivering the process status reports intelligible to the plant operators so as to prevent the tragic consequences of process failures. In this context, several businesses in the automation industry, including ABB, Honeywell, and Siemens, have developed Controller Performance Monitoring (CPM) as part of process diagnostic systems. Notably, the methodologies utilised are tending to be primarily data-driven, emphasising the significance of avoiding the use of model-based procedures, which are impractical for real-world commercialisation. This is also supported by huge corporations' desire to use widely available data from their data acquisition and control systems in order to step into the Industry 4.0 era.

Therefore, researchers have made great efforts to develop techniques that only use routine data to detect controller-related malfunctions. Oscillations are the most noticeable feature that is undesirable and needs to be investigated. Oscillation detection in the literature was addressed in two aspects: single-loop and plant-wide (Bounoua et al., 2022). From the earliest attempts by Horch (1999) to detect valve stiction in individual loops using the cross-correlation function (CCF) until today, new approaches are continuously being proposed either to improve the performance of existing methods or to tackle the common issues encountered in practical applications that have not been addressed before. ACF, presented by Thornhill et al. (2003), has been intensively used in combination with other methods to detect the presence of oscillation by checking the regularity of zero-crossings (Srinivasan and Rengaswamy, 2012; Guo et al., 2014a; Naghoosi and Huang, 2014). However, this method is not robust to coloured noise as well as non-stationary and multiple oscillatory signals. More attention has recently been paid to decomposition techniques in order to extract the components that arise in measurements undergoing multiple oscillations. These include the Empirical Mode Decomposition (EMD), which extracts Intrinsic Mode Functions (IMF) based on the Huang–Hilbert transform. The conventional form of EMD showed a deficiency in distinguishing between significant oscillatory components induced by actual disturbances and components associated with noise. Srinivasan et al. (2007) proposed a modified version to deal with this problem by mean-shifting the signal. Another alternative was proposed by Aftab et al. (2018) based on noise incorporation. However, these methods

* Corresponding author.
E-mail address: wahiba.bounoua@uia.no (W. Bounoua).

https://doi.org/10.1016/j.compchemeng.2023.108173
Received 7 November 2022; Received in revised form 31 January 2023; Accepted 8 February 2023
Available online 10 February 2023

may suffer from mode-mixing and end-effect problems. Using a similar principle to EMD, a Local Mean Decomposition (LMD) was proposed by Lang et al. (2016), which sets the number of extracted modes *a priori* to two. A Chirp Mode Decomposition (CMD) was also proposed in an adaptive approach, using an energy ratio to extract significant components (Chen et al., 2019, 2020a). However, this method cannot handle data corrupted by coloured noise as well, and intermittent oscillations were not investigated. All the aforementioned methods operate in an offline mode. Intrinsic Time-scale Decomposition (ITD) was presented by Guo et al. (2014b) and Xie et al. (2016) to detect oscillations in an online mode. However, this approach is complex and requires iterative and repeated extrema evaluations in order to detect the presence of oscillations. Moreover, this method can only handle white noise, whereas the presence of coloured noise may deteriorate the monitoring results. Discrete Cosine Transform (DCT) has been developed by Li et al. (2010). The underlying notion behind DCT is that various frequency components occupy different areas in the transformed space. Therefore, the inverse DCT (iDCT) must also be applied to transform the signal back to the time domain after decomposition. The online version proposed by Wang et al. (2013) uses an adaptive window size to capture new oscillatory patterns if oscillations were not detected in previous windows. As a result, this technique will recursively detect oscillation, making immediate detection difficult. Furthermore, this method extracts only one dominant oscillating frequency, which means it cannot handle multiple oscillations. Another method called the Variational Mode Decomposition (VMD) selects only one significant principal component to interpret the oscillations of the variables rather than decomposing the time series into multiple oscillating modes, which also cannot deal with multiple oscillations (Wardana, 2015).

Even though the Wavelet Transform (WT) is regarded as a strong tool in oscillations analysis, it has only been employed in a few research works and within a limited context. Moreover, WT is one of the few methods available in the literature that has been used for real industrial packages, such as the industrial integrated tool named Time2Wave proposed by Matsuo et al. (2004) and created by Yamatake Corporation and Mitsui Chemicals. However, the use of WT was straightforward and required human interaction. An alternative automatic WT-based framework has been presented by Guo et al. (2014a) by analysing binary colourmap images generated through the Continuous WT (CWT); this method has shown satisfactory results. However, it required preprocessing to deal with noise using the Discrete WT (DWT).

In fact, measurements from even basic dynamical systems can exhibit complex characteristics, rendering linear correlations futile. The irregular behaviour of realistic time series can be linked to two distinct factors: (i) the explicit random fluctuations acting on the process from external sources, identified as noise, which might be white or coloured, and time-varying disturbances; and (ii) coherent fluctuations caused by the emergence of a genuine fault. The latter is usually contaminated with noise, making the detection process even more difficult. Consequently, a data-driven algorithm that can distinguish between these two cases is highly desirable. This paper proposes a new online controller faults detection technique that can successfully detect the occurrence of oscillatory faults. The real-time monitoring is achieved by introducing a new detection statistic constructed based on the powerful Detrended Fluctuation Analysis (DFA) technique. Recently, DFA was utilised as only a denoising approach in the preprocessing stage of a causality analysis using Convergent Cross Mapping (CCM) (Chen et al., 2020b). However, its potential for expressing the complexity of signals has not been examined earlier for real-time fault detection. Hence, this paper uses DFA as the main fault detection method cast in a sliding window paradigm. This method has the advantage over the previously stated methods regarding straightforward online detection; as new observations emerge, it can report the degradation after their occurrence and determine the duration of persistent and/or intermittent oscillations. Furthermore, it has the ability of detecting incipient faults at their earliest appearance. Detecting such slow drifts in process operations has yet to be addressed. This gives the proposed approach the important advantage of indicating future problems relevant to predictive maintenance. As mentioned earlier, previously proposed decomposition-based online detection methods had to re-evaluate the old observations when multiple/intermittent oscillations were detected. Indeed, decomposing the signal in real-time is unreliable since multiple intermittent oscillations will lead to spurious results, and the recursion, in this case, will further increase the computational complexity.

Non-stationarity, intermittency, nonlinearity, time-variability, and multiple oscillations are characteristics of signals that have been addressed individually in the literature. Thus, most of the data-driven strategies proposed in the literature lack flexibility and generality. DFA assesses the intrinsic self-affinity and the nonlinear correlation features of dynamical systems, which require no *a priori* assumptions about the signal's characteristics such that short- and long-range correlations inherent in non-stationary time-variant trends can be adequately captured (Kantz and Schreiber, 2003). The key contribution of this paper is to exploit these important properties to make the first detection stage automatic and independent of any assumptions regarding the system. The online monitoring accomplished using the novel detection statistic is followed by an improved decomposition method named Empirical Wavelet Transform (EWT) (Gilles, 2013) to extract the oscillating modes and further deal with multiple oscillations. Unlike existing detection methods, the decomposition is not performed unless oscillations are detected. EWT has been proven to outperform EMD, and VMD (Wardana, 2016). However, the number of extracted components using these methods, including EWT is still an unresolved problem. As can be seen from the earlier discussions, the decomposition is either carried out until the signal is over-decomposed, resulting in multiple insignificant components or the number of modes is fixed prior to the analysis, which imposes a constraint in case of multiple oscillations exceeding the pre-defined number (Dragomiretskiy and Zosso, 2014). The Pearson correlation coefficient has mostly been used in combination with these methods to detect the significant modes when the signal is over-decomposed. However, it is more appropriate to identify the significant modes that originally constructed the underlying time series by considering nonlinear correlations. Another recent index that is found in the literature is the Energy Ratio (ER) built on the spectrum content of white noise (Chen et al., 2019). Any noise signal whose power spectrum is a function of frequency is referred to as coloured noise (Zhivomirov, 2018) where ER is not applicable; the ER, in this case, will result in inaccurate decomposition. Moreover, the methods proposed to segment the power spectrum in EWT result in an incorrect decomposition in the presence of the near-in-frequency multiple components; this requires the tuning of multiple parameters (Amezquita-Sanchez and Adeli, 2015; Zheng et al., 2017; Hu et al., 2017; Zhuang and Liao, 2020). Based on such considerations and using the potentials proved in the first phase of this work of DFA in characterising noise of any nature and oscillatory signals, an Improved EWT (IEWT) is proposed by evaluating the residuals and the significance of extracted modes after each decomposition step using DFA. This ensures that the exact number of oscillatory components is extracted without any user presumptions and, more importantly, overcomes the over-decomposition problem. The combination of these two stages increases the overall reliability and accuracy of the suggested approach, allowing it to function in real-time for any process characteristics. In order to check the efficiency of the proposed framework, the algorithm is examined on simulated data and industrial case studies. Its sensitivity to abnormal behaviours is assessed by considering common phenomena in routine industrial data.

The remaining of this paper is organised as follows: Sections 2 and 3 introduces the different bases techniques and methodologies employed in the proposed work. Section 4 describes the DFA-IEWT framework. Section 5 presents the application results. Simulated case studies are represented and discussed in Section 6. Section 7 is the implementation of the proposed paradigm on industrial case studies. Finally, a conclusion is reported in Section 8.

2. Detrended fluctuation analysis

DFA developed by Peng et al. (1994) quantifies dependencies between intervals in time series derived from dynamical systems. The fundamental measure of complexity in time series is the Hurst exponent which is widely known as a parameter that reflects temporal correlations based on self-similarity (Hurst, 1951). However, due to its theoretical background, the presence of strong trends leads to inaccurate parameters. A nonstationary signal is characterised by trends where its distribution is time-variant, i.e. the shift in time of the signal changes the joint distributions of its instances. This can also be observed from the variability in time of its mean, standard deviation, moments, joint moments, and the correlation functions. DFA detects long-range correlations inherent in a seemingly nonstationary time series while simultaneously avoiding the false detection of apparent long-range correlations caused by significant trends (Peng et al., 1995). Hence, to deal with these non-stationarities, a bounded signal under analysis must first be converted into an unbounded process which can be seen as a diffusion-like process. This conversion can be achieved through the following equation (Kantz and Schreiber, 2003):

$$\mathfrak{P}(t) = \int_0^t (\mathbf{x}(\tau) - \langle \mathbf{x} \rangle)\, d\tau \tag{1}$$

For a given time series $\mathbf{x}(t) \in \Re$ and its whole range mean:

$$\langle \mathbf{x} \rangle = \frac{1}{T} \int_0^T \mathbf{x}(t)\, dt \tag{2}$$

This transforms the original signal into the signal profile, which is the integrated signal with the offset eliminated. In practice, this is computed as an averaged cumulative sum. The fluctuation analysis is then performed on interevent intervals of $\mathfrak{P}(t)$ and detrending is carried out through subtraction in the temporal segments. This is achieved by introducing polynomials of order l in the form of $\mathcal{P}_v^{(l)}(z,t,\tau,\Delta) = \sum_{i=0}^{l} a_i z^i$ and smoothing over the interval $\{\mathfrak{P}(\tau)\}_t^{t+\Delta}$ by solving the following for the polynomial coefficients:

$$\arg\min_{\mathcal{P}_v^{(l)}} \int_t^{t+\Delta} \left(\mathcal{P}_v^{(l)}(z,t,\tau,\Delta) - \mathfrak{P}(\tau)\right)^2 d\tau \tag{3}$$

which minimises the fitting error in the least squares sense over the time scale Δ. The fluctuations are estimated as the root-mean-square deviation from the trend as:

$$v^{(l)}(\Delta) := \frac{1}{\Delta} \int_t^{t+\Delta} \left(\mathcal{P}_v^{(l)}(z,t,\tau,\Delta) - \mathfrak{P}(\tau)\right)^2 d\tau \tag{4}$$

This is computed over the entire time series and correspondingly repeated with different time scales Δ. The scaling exponent denoted α was found to behave as a power law of Δ according to the following relation:

$$\left\langle v^{(l)}(\Delta) \right\rangle \propto \Delta^{\alpha} \tag{5}$$

where $\left\langle v^{(l)}(\Delta) \right\rangle$ is the average taken for the whole time series. The plot $\log(v^{(l)}(\Delta))$ versus $\log(\Delta)$ tends then to have a linear part obeying the above-mentioned power law. The slope of this part is the scaling exponent α.

3. Empirical Wavelet Transform

EWT extracts the time-domain intrinsic modes derived from the distinctive frequency-domain components through spectrum segmentation. In fact, EWT is an improved version of EMD which combines the potentials of the Wavelet Transform (WT) due to its strong theoretical background and the adaptability of EMD which gives more reliable decomposition.

The advantage of WT is that it can analyse non-stationary signals using both the CWT and DWT forms which carry out a multiresolution analysis. CWT calculates the correlation between the time series and the so-called mother wavelet function ψ as follows (Chandrasekhar et al., 2013; Ahad and Ahmed, 2021):

$$\mathbf{X}_{\mathrm{CWT}}(a,b) = \frac{1}{\sqrt{a}} \int_{-\infty}^{+\infty} \mathbf{x}(t) \psi^* \left(\frac{t-b}{a}\right) dt \tag{6}$$

where * indicates the complex conjugate of the wavelet, a represents the scale parameter, and b is the translation parameter. CWT computes the wavelet coefficients $\mathbf{X}_{\mathrm{CWT}}$ by shifting and compressing/expanding the wavelet function that introduces a time–frequency resolution analysis. In contrast, DWT decomposes the signal into its low-frequency component and its high-frequency component by using the scaling function φ (also called father wavelet) and the mother wavelet ψ as:

$$\mathbf{x}(t) = \sum_{k=-\infty}^{\infty} c_k \varphi(t-k) + \sum_{k=-\infty}^{\infty} \sum_{j=0}^{\infty} d_{j,k} \psi\left(2^j t - k\right) \tag{7}$$

where c_k and $d_{j,k}$ are the low-pass and high-pass coefficients, respectively.

The main drawback of WT is the requirement to predefine the wavelet basis with fixed mother and father wavelets regardless of the processed signal. The adaptability of EWT is achieved by considering the location of the information contained in the spectrum using the Fourier basis, which allows the construction of a more consistent filter bank.

This filter bank is a sequence of bandpass filters on the segments $\{\Lambda_k\}_{k=1}^{K}$ of the power spectrum with boundaries $[w_{k-1}, w_k]$. Only the non-negative normalised frequencies are considered since the processed signals are real with symmetric spectrum, making the segments lie in the range $[0,\pi]$ which satisfy $\bigcap_{k=1}^{K} \Lambda_k = [0,\pi]$. The empirical scaling functions $\widehat{\varphi}(\omega)$ and the empirical wavelets $\widehat{\psi}(\omega)$ are then obtained as:

$$\widehat{\varphi}_k(\omega) = \begin{cases} 1; \\ \text{if } |\omega| \le (1-\gamma)\omega_k \\ \cos\left[\frac{\pi}{2}\beta\left(\frac{1}{2\gamma\omega_k}\left(|\omega| - (1-\gamma)\omega_k\right)\right)\right]; \\ \text{if } (1-\gamma)\omega_k \le |\omega| \le (1+\gamma)\omega_k \\ 0; \\ \text{otherwise} \end{cases} \tag{8}$$

$$\widehat{\psi}_k(\omega) = \begin{cases} 1; \\ \text{if } (1+\gamma)\omega_k \le |\omega| \le (1-\gamma)\omega_{k+1} \\ \cos\left[\frac{\pi}{2}\beta\left(\frac{1}{2\gamma\omega_{k+1}}\left(|\omega| - (1-\gamma)\omega_{k+1}\right)\right)\right]; \\ \text{if } (1-\gamma)\omega_{k+1} \le |\omega| \le (1+\gamma)\omega_{k+1}, \\ \sin\left[\frac{\pi}{2}\beta\left(\frac{1}{2\gamma\omega_n}\left(|\omega| - (1-\gamma)\omega_k\right)\right)\right]; \\ \text{if } (1-\gamma)\omega_k \le |\omega| \le (1+\gamma)\omega_k, \\ 0; \\ \text{otherwise} \end{cases} \tag{9}$$

where γ is defined later in Eq. (13) and the function $\beta(\varrho)$ is an arbitrary function belonging to the space $C^m[(0,1)]$ which must comply with the following conditions:

$$\beta(\varrho) = \begin{cases} 1 & \text{if } \varrho \ge 1 \\ 0 & \text{if } \varrho \le 0 \\ \beta(\varrho) + \beta(1-\varrho) = 1 & \text{if } \forall \varrho \in [0,1] \end{cases} \tag{10}$$

for $\varrho = \frac{1}{2\gamma\omega_k}\left(|\omega| - (1-\gamma)\omega_k\right)$. From the wide variety of functions satisfying these properties, the one adopted here is selected due to its popularity in the literature that is given as:

$$\beta(\varrho) = \varrho^4\left(35 - 84\varrho + 70\varrho^2 - 20\varrho^3\right) \tag{11}$$

The parameter γ is defined to ensure no significant overlapping between two adjacent transition bands so that the set $\left\{\phi_1(t), \{\varphi_k(t)\}_{k=1}^{K}\right\}$ is a tight frame of $L^2(\Re)$, meaning that:

$$\sum_{s=-\infty}^{+\infty}\left(\left|\widehat{\varphi}_1(\omega+2s\pi)\right|^2+\sum_{k=1}^{K}\left|\widehat{\psi}_k(\omega+2s\pi)\right|^2\right)=1 \tag{12}$$

which holds for:

$$\gamma<\min_k\left(\frac{\omega_{k+1}-\omega_k}{\omega_{k+1}+\omega_k}\right) \tag{13}$$

EWT is then defined through the coefficients $W_f^{\varepsilon}(k,t)$ using the inner product as:

– Detail coefficients:

$$W_f^{\varepsilon}(k,t)=\int f(\tau)\overline{\psi_k(\tau-t)}\mathrm{d}\tau \tag{14}$$

And through the Inverse Fast Fourier Transform (IFFT) using the frequency-domain representation as:

$$W_f^{\varepsilon}(k,t)=\left(\widehat{f}(\omega)\overline{\widehat{\psi}_k(\omega)}\right)^{\vee} \tag{15}$$

– Approximation coefficients:

$$W_f^{\varepsilon}(0,t)=\int f(\tau)\overline{\varphi_1(\tau-t)}\mathrm{d}\tau=\left(\widehat{f}(\omega)\overline{\widehat{\varphi}_1(\omega)}\right)^{\vee} \tag{16}$$

The reconstruction of the signal is obtained as follows:

$$\begin{aligned}\mathbf{x}(t)&=W_f^{\varepsilon}(0,t)\varphi_1(t)+\sum_{n=1}^{N}W_f^{\varepsilon}(n,t)\psi_n(t)\\&=\left[\widehat{W}_f^{\varepsilon}(0,\omega)\widehat{\varphi}_1(\omega)+\sum_{n=1}^{N}\widehat{W}_f^{\varepsilon}(n,\omega)\widehat{\psi}_n(\omega)\right]^{\vee}\end{aligned} \tag{17}$$

Which can be expressed as:

$$\mathbf{x}(t)=f_{c_0}(t)+\sum_{k=1}^{K}f_{c_k}(t) \tag{18}$$

Therefore the components $\{f_{c_k}(t)\}_{k=0}^{K}$ are defined as:

$$f_{c_0}(t)=W_f^{\varepsilon}(0,t)*\varphi_1(t) \tag{19}$$

$$f_{c_k}(t)=W_f^{\varepsilon}(k,t)*\psi_k(t) \tag{20}$$

4. DFA-IEWT proposed method

The general framework of the proposed method is depicted in Fig. 1. In this structure, the first phase of the detection scheme is accomplished by designing a new detection index using DFA named $\mathrm{DI_{DFA}}$. The signals confirmed to be derived from a faulty control system are then put into the second phase of this hierarchical detection system, where characteristics of the oscillations are further investigated using IEWT. the procedure is outlined in detail in the following subsections:

4.1. Online monitoring phase

The scaling exponent quantifying the time trends fluctuations is computed for the discrete signals under analysis sampled from real processes measurements. For a given signal $\mathbf{x}\in\Re^N$, a moving window is constructed as follows:

$$\{\mathbf{w}_t\}_{t=1}^{N-p+1}=\{\mathbf{x}(t)\ \mathbf{x}(t+1)\cdots\mathbf{x}(t+p-1)\}_{t=1}^{N-p+1} \tag{21}$$

where p is the size of the window. On this data window, we define a set of M equally spaced time scales $\Xi=\{\Delta_j : j=1,2,\ldots,M\}$ on the logarithmic scale with a lower bound of four samples and the length of the window as the upper bound. The $\mathrm{DI_{DFA}}$ is thereafter computed as:

1. The signal profile is computed by Eq. (1) as Hardstone et al. (2012):

$$\mathfrak{P}(i)=\sum_{\mathrm{n}=1}^{i}\mathbf{w}_t(\mathrm{n})-\langle\mathbf{w}_t\rangle \tag{22}$$

2. Starting with the lowest time scale $\Delta_j\in\Xi$ for $j=1$, the time window signal profile $\mathfrak{P}$ is split into D blocks $\{\mathfrak{P}_d\}_{d=1}^{D}$ of length Δ_j with 50% overlap which increases the number of blocks and ultimately improves performance.
   i. A polynomial of order l (Eq. (3)) is fit to the block $\mathfrak{P}_d$ and the trend is removed by subtracting the fit from the time series to construct the detrended signal $\mathfrak{P}_d^{det}$.
   ii. The fluctuations are then computed as the standard deviation of $\mathfrak{P}_d^{det}$ for Eq. (4) which is given as:

$$\sigma\left(\mathfrak{P}_d^{det}\right)=\sqrt{\frac{\sum_{i=1}^{\Delta_j}\left(\mathfrak{P}_d^{det}(i)-\langle\mathfrak{P}_d^{det}\rangle\right)^2}{\Delta_j}} \tag{23}$$

3. Steps (i and ii) are repeated for all $\{\mathfrak{P}_d\}_{d=1}^{D}$ and the fluctuation function is then computed as the mean of the standard deviation of all blocks as:

$$F\left(\Delta_j\right)=\langle\sigma\left(\mathfrak{P}_d^{det}\right)\rangle \tag{24}$$

4. Steps 2–3 are repeated for all time scales $\Xi=\{\Delta_j : j=1,2,\ldots,M\}$ giving a set of fluctuation points $\{F\left(\Delta_j\right)\}$.
5. Making use of all the possible values Δ_j within the time window under investigation results in M pairs of $\left(log\left(\Delta_j\right), log\left(F\left(\Delta_j\right)\right)\right)$ used to depict the $log-log$ plot. This ensures that sufficient amount of information is explored about the intrinsic properties of the temporal data.
6. At this stage, $\mathrm{DI_{DFA}}$ is computed as the slope of the linear trend line corresponding to the pertinent range of spatial time scales and can be estimated by means of linear regression methods.
7. Eventually, a decision rule is constructed in order to assess whether the process is operating under healthy mode or is affected by an abnormal event as:

$$\begin{cases}\mathcal{H}_0 : DI_{DFA}\le J_{th,DI_{DFA}}\\ \mathcal{H}_a : DI_{DFA}>J_{th,DI_{DFA}}\end{cases} \tag{25}$$

   where $J_{th,DI_{DFA}}$ is the threshold established such that instances of DI_{DFA} must remain within a defined allowable limit if the process is in the normal mode; the detection statistic is said to be in the non-significance region and null hypothesis $\mathcal{H}_0$ is accepted. Otherwise, $\mathcal{H}_0$ is rejected and the alternative hypothesis $\mathcal{H}_a$ is accepted if any point exceeds this threshold and appears to reside in the critical region. Oscillatory behaviour in the control loop measurements is then detected, and the process is judged to be out-of-control. This threshold is selected based on the long-term and short-term fluctuations present in the data, which will be discussed in Section 5.
8. This procedure (steps 1–7) is implemented at each time index t; the new operating data observation is incorporated into the sliding window while discarding old insignificant observations, resulting in a new value of the test statistic DI_{DFA} used for online status assessment of the control loop.

4.2. Improved EWT for oscillations characterisation phase

It is essential to design a filter bank that can appropriately extract only the significant elements and automatically discard the spurious and noisy components in order for a signal decomposition technique to isolate the individual components of the original abnormal signal reliably. EWT is an effective technique that possesses the adaptability

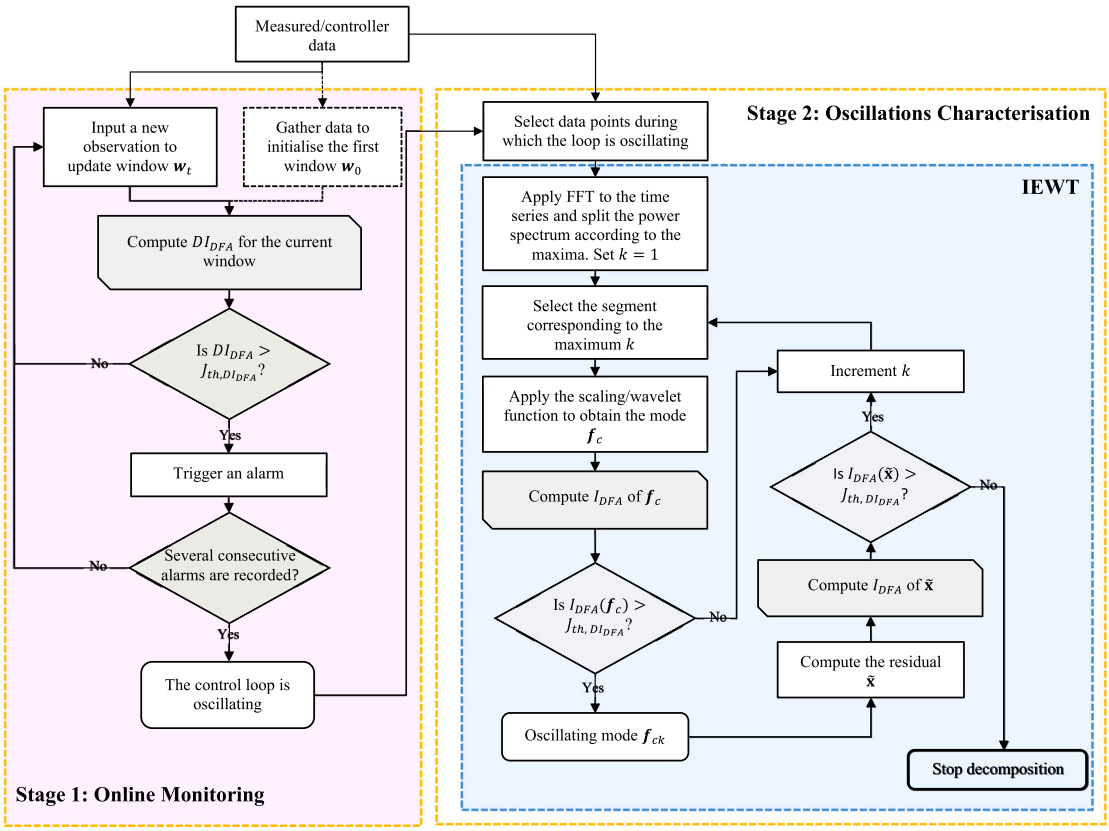

Fig. 1. Workflow diagram of the proposed DFA-IEWT-based controller performance monitoring algorithm.

property, allowing it to separate the Fourier supports according to their power spectrum strength. However, this method can work efficiently only if the signal has well-separated frequency components. The mode mixing problem is frequently caused by the existence of a signal trend, near-in-frequency oscillating components, or noise, especially for small sample-size signals.

To this end, the capability of DFA to distinguish between the fluctuations stemming from significant oscillations and noise is used to extract the oscillating modes in an adaptive manner. This can be achieved through the following procedure:

1. Obtain the frequency spectrum of the raw signal detected to be oscillating from the first phase using FFT.
2. Detect the local maxima and set the boundaries as the midpoint between consecutive maxima.
3. For the segment containing the maximum power:
   i. Based on the location of the selected segment, apply either the scaling function or the empirical wavelets (Eqs. (8) and (9)) and obtain f_c;
   ii. Compute the DFA index I_{DFA} (computed in a similar manner to DI_{DFA}) of the extracted component;
   iii. If its associated I_{DFA} exceeds the threshold, the component is considered significant and designated as oscillatory. Otherwise, it is inferred that the component was retrieved from a noisy segment.
   iv. The residual is then obtained by subtracting the significant components from the signal, and the corresponding I_{DFA} is computed to appraise whether the residual contains significant oscillations. The components arising from noise are not included in the residual calculations in order not to affect the frequency content.
4. The next maximum is identified and Step 3 is repeated.

The procedure is stopped when the I_{DFA} of the residual falls below the threshold, indicating that all oscillating components have been extracted. The practical computations are presented in detail in Algorithm 1, and the framework is summarised in Algorithm 2.

5. Application

This section presents an application of the proposed framework to controller performance monitoring. In order to illustrate the advantages of integrating EWT with DFA, as a tool to express the complexity of the time series with respect to its linear and/or nonlinear behaviour, the developed methodology is tested on a wide range of normal as well as oscillatory signals using simulated signals, a simulated First Order with Time Delay (FOTD) SISO process, and industrial case studies.

5.1. Performance evaluation criteria

Since the fault detection is implemented in real-time during the first phase, the statistical framework for evaluating the performance efficiency of the DFA-based monitoring is constructed through a detection index analysis including: (i) the fault Detection Latency (DL), reflecting the pace of reactivity of the detection system to faults after they occur, (ii) the False Alarm Rate (FAR) which quantifies the system's robustness and stability in the face of uncertainty and is calculated as the probability of type I error, and (iii) the Fault Detection Rate (FDR), characterising the sensitivity of the control chart to severities evaluated as the power of the test (Aldrich and Auret, 2013; Ding, 2014). These indices are appraised for different data sets containing the fault-free operation part associated (accepting $\mathcal{H}_0$) and faulty condition part (accepting $\mathcal{H}_a$) as:

– The probability of false alarm (P_{FA})

$$P_{\text{FA}} = P(DI_{DFA} > J_{th,DI_{DFA}} \mid \mathcal{H}_0) \tag{26}$$

Algorithm 1: The proposed IEWT algorithm

Data: Input vector $\mathbf{x}$
Result: Oscillating modes $\{\boldsymbol{f}_{ck}\}_{k=1}^{K}$
$\tilde{\mathbf{x}} \leftarrow \mathbf{x}$;
$k \leftarrow 1$;
Step 1: Compute FFT of the raw data vector $\mathbf{x}$ and detect local maxima;
Step 2: Split the Fourier supports into l segments in the range $[0 \ \ \pi]$ according to the maxima;
while $I_{DFA}(\tilde{\mathbf{x}}) \geq J_{th,DI_{DFA}}$ **do**
  Obtain the boundaries of the Fourier segment with the next maximum power spectrum;
  if *the first segment is extracted* **then**
    Compute the EWT Meyer scaling function using Eq. (8);
    Obtain $\boldsymbol{f}_c$ using IFFT in Eq. (19);
  else
    Compute the EWT Meyer wavelet function using Eq. (9);
    Obtain $\boldsymbol{f}_c$ using IFFT in Eq. (20);
  end
  compute $I_{DFA}(\boldsymbol{f}_c)$;
  if $I_{DFA}(\boldsymbol{f}_c) \geq J_{th,DI_{DFA}}$ **then**
    The extracted component is significant: $\boldsymbol{f}_{ck} \leftarrow \boldsymbol{f}_c$;
    The residual is computed: $\tilde{\mathbf{x}} = \tilde{\mathbf{x}} - \boldsymbol{f}_{ck}$;
    Compute $I_{DFA}(\tilde{\mathbf{x}})$;
    Set k=k+1;
  else
    discard $\boldsymbol{f}_c$ as being noise;
  end
end
K=k;
The set $\{\boldsymbol{f}_{ck}\}_{k=1}^{K}$ is taken as the oscillating modes of the original signal.

Algorithm 2: The proposed DFA-based IEWT detection algorithm

Data: Input vector $\mathbf{x} \in \Re^N$
Result: Online detection alarm chart and oscillating modes $\{\boldsymbol{f}_{ck}\}_{k=1}^{K}$

Step 1: Set $t = 1$;
repeat
  Step 2: From the time series $\mathbf{x}(t)$ obtain the time window frame $\mathbf{w}_t$ using Eq. (21);
  Step 3: Generate the signal profile $\mathfrak{P}$ using Eq. (22) and the set $\{\Delta_j \in \Xi\}$;
  Step 4: Set $j = 1$ and $\Delta_j = 4$;
  repeat
    Step 5: Set $i = 1$, $d = 1$, and $s = \lceil \Delta_j/2 \rceil$;
    while $(i + s) \leq p$ **do**
      Step 6: Find the least-squares fit in this d^{th} block of Δ_j values of $\{\mathfrak{P}\}$;
        $\mathcal{P}_v^{(l)}(z,t,\tau,\Delta_j) = \sum_{i=0}^{l} a_i z^i$;
      Step 7: Subtract the fit from the signal profile ;
        $\mathfrak{P}_d^{det} = \{\mathcal{P}_v^{(l)}(z,t,\tau,\Delta_j) - \mathfrak{P}(\tau)\}_{\tau=i}^{\Delta_j+i-1}$;
      Step 8: Take the standard deviation of this detrended signal;
        $\sigma(\mathfrak{P}_d^{det}) = \sqrt{\frac{\sum_{i=1}^{\Delta_j}\left(\mathfrak{P}_d^{det}(i) - \langle\mathfrak{P}_d^{det}\rangle\right)^2}{\Delta_j}}$;
      Step 9: Increment the block starting index: $i = i + s$;
      Step 10: Increment the block index: $d = d + 1$;
    end
    Step 11: Set $D = d$;
    Step 12: Average all values of the standard deviation;
      $F(\Delta_j) = \frac{1}{D}\sum_{d=1}^{D}\sigma(\mathfrak{P}_d^{det})$;
    Step 13: Increase the time scale Δ_j by incrementing $j = j + 1$;
  until $j = M$;
  Step 14: Report $\{\Delta_j\}_{j=1}^{M}$ and $\{F(\Delta_j)\}_{j=1}^{M}$;
  Step 15: plot $log(\Delta_j)$ vs. $log(F(\Delta_j))$;
  Step 16: The slope of the linear trend is then the detection index $\mathrm{DI}_{\mathrm{DFA}}(t)$ at instance t;
  Step 17: Increment the window index: $t = t + 1$;
until $t = N - p + 1$;
Step 17: Implement Algorithm 1 for the signals reported to be oscillating according to the decision rule in Eq. (25) to obtain the oscillating modes $\{\boldsymbol{f}_{ck}\}_{k=1}^{K}$.

– The probability of fault detection (P_{FD})

$$P_{\mathrm{FD}} = P(DI_{DFA} > J_{th,DI_{DFA}} \mid \mathcal{H}_a) \tag{27}$$

5.2. Parameters tuning

The premise behind employing a moving window in the controller degradation detection system is to conduct the analysis in real-time by removing old observations from the data window and embedding new ones to iteratively update the calculations of the fault indicator DI_{DFA}. To properly set the window size, several simulated case studies in both the healthy and oscillatory modes were utilised to assess the influence of the window size on the detection efficiency. However, the threshold $J_{th,DI_{DFA}}$ needs first to be selected in order to derive these probabilities.

5.2.1. Threshold computation

Time series can be regarded as self-affine, with self-affinity defined as exhibiting statistical self-similarity. In this respect, time series are considered a composition of statistically identical replicas of the whole signal, which can be transformed into a series of sine waves of varying frequencies (Riley et al., 2005). Considering the frequency domain representation, a time series with a single oscillatory component will have a single distinguished spike in its power spectrum. In contrast, spikes at certain frequencies will appear in a time series encompassing multiple components with varying amplitudes reflecting their power strength and the degree of dominance. Real measurements are typically corrupted by noise, either white or coloured. Therefore, the power spectrum of measurement under normal conditions without oscillations will be similar to that of noise. White noise has a flat spectrum with equal energy at all frequencies, making only the high-frequency fluctuations discernible in the signal. Coloured noise exhibits less energy at specific frequency ranges than white noise. However, no distinct spikes can be found (Turcotte, 1997).

The temporal correlation may also explain these inferences within the signal under examination since the autocorrelation function is obtained as the inverse Fourier transform of the power spectrum, where a noisy non-oscillatory time series results in an exponentially decaying autocorrelation function. The ACF decay ratio has previously been used to detect the existence of oscillations in control loops (Miao and Seborg, 1999). However, ACF can only be applied to stationary data. DFA has the advantage of quantifying the temporal correlation for even non-stationary signals and requires no *a priori* assumptions about the data. From the perspective of the DFA, regular signals contaminated by white noise are recognised by samples that are uncorrelated with preceding values. In contrast, the presence of coloured noise will result in either a short-term or long-term correlation; in both cases, it will exhibit $DI_{DFA} \leq 1$. When the signal showed a more persistent long-term correlation, it was found that DI_{DFA} diverges from 1, which is the case proven to follow a Brownian motion that possesses an

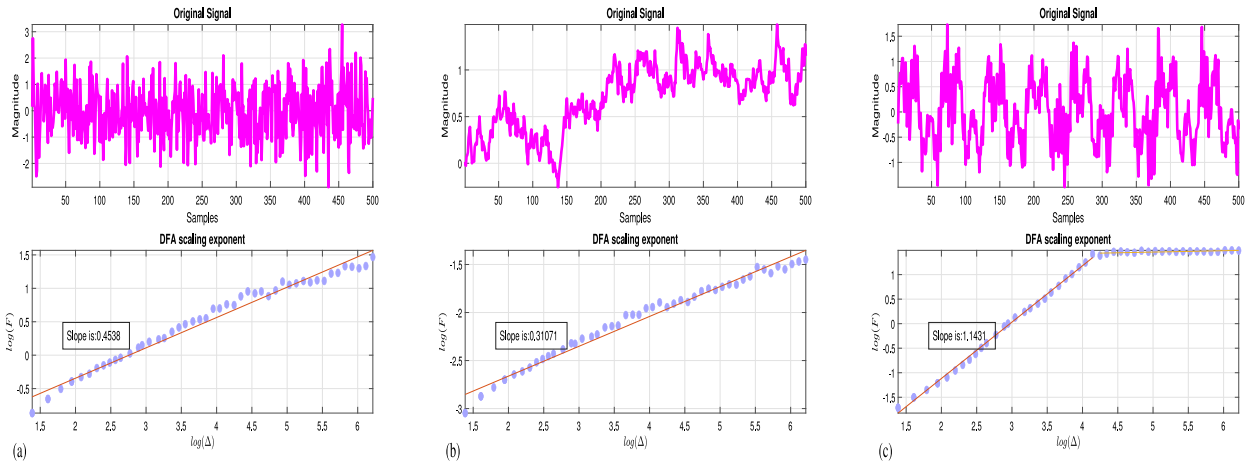

Fig. 2. DFA for (a) stationary white noise, (b) non-stationary coloured noise, and (c) oscillatory time series evaluated as the slope of the linear part of $log\,(F\,(\Delta))$ vs. $log\,(\Delta)$ to illustrate the threshold selection basis.

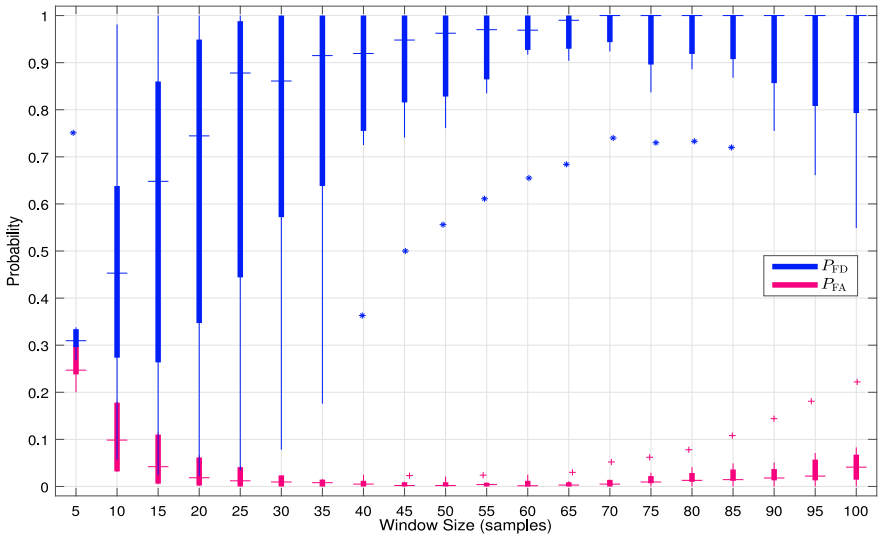

Fig. 3. The effect of changing the window size on P_{FD} and P_{FA} for simulated normal and oscillatory signals corrupted by different levels of noise.

oscillatory characteristic (Kantz and Schreiber, 2003; Lejay and Pigato, 2017). DI_{DFA} can also be viewed as an indicator of the scale at which the fluctuations appear; rough fluctuations at small scales are generally caused by noise but without an obvious degradation in the controller performance. Nevertheless, the coherent fluctuations on the larger scales are induced by the onset of a genuine fault. As a result, a threshold $J_{th,DI_{DFA}} = 1$ is set in order to make the decision on the state of the controller. This can be shown through simulated case studies. Fig. 2 illustrates that DFA takes values below the selected threshold for normal signals and diverges significantly for the degraded and oscillating signal.

5.2.2. Window size selection

The decision rule based on this threshold was used to select the appropriate window size. Several simulated signals, incorporating different healthy and faulty states corrupted by white or coloured noises, were embedded into the DFA-based detection system with varying window sizes. Accordingly, P_{FA} and P_{FD} were evaluated for each corresponding case study, and Fig. 3. shows the effect of the window size on these evaluation indices. It is clear that small window sizes result in an appalling performance, especially when $p = 5$ with a high number of false alarms and a poor fault detection rate; this result was expected since the minimum time scale is selected as $\Delta_1 = 4$, implying that very few pairs of $\left(log\left(\Delta_j\right), log\left(F\left(\Delta_j\right)\right)\right)$ are utilised for the scaling exponent computations; hence, there is insufficient information for further exploration of the signal complexity. As the window size increases, P_{FA} decreases significantly, reaching approximately zero, whereas P_{FD} increases to up to one for the majority of the cases under examination. However, as the window size increases beyond 70, the monitoring system exhibits relatively increased missed detection instances. This can be explained as the long-term correlation computations might deteriorate for larger sample sizes. Consequently, the window size $p = 70$ is selected for the remainder, achieving the best trade-off between P_{FA} and P_{FD}. Nevertheless, the practitioners might increase the window size if the process is perceived to be slow with a small sampling time to capture the oscillations since the size does not affect FAR significantly. This ensures that sufficient information is explored about the intrinsic properties of the data within the temporal frame.

6. Case study 1: Simulated examples

First, the proposed DFA-IEWT framework is tested on simulated case studies to verify its efficiency in distinguishing between normal and oscillatory signals corrupted by different levels of white and coloured noise. The proposed online paradigm was implemented for non-oscillatory and oscillatory signals in the scenarios discussed below:

Table 1
FAR results for the online monitoring of the non-oscillatory simulated case studies with varying variances of the white noise.

Noise type	Variance	0.2		0.4		0.6		0.8		1		1.2		1.4		1.6	
		St.	N.St	St.	N.St	St.	N.St	St.	N.St	St.	N.St	St.	N.St	St.	N.St	St.	N.St
	White noise	0.000	0.000	0.055	0.017	0.012	0.018	0.000	0.030	0.000	0.016	0.018	0.010	0.004	0.012	0.006	0.011
Coloured noise filtering transfer function	$H(z) = \frac{1}{1+0.5z^{-1}}$	0.007	0.019	0.000	0.041	0.002	0.061	0.000	0.067	0.000	0.045	0.007	0.051	0.006	0.043	0.009	0.013
	$H(z) = \frac{1-0.2z^{-1}}{1-0.1z^{-1}+0.8z^{-2}}$	0.000	0.000	0.000	0.017	0.000	0.007	0.000	0.005	0.000	0.000	0.000	0.000	0.000	0.000	0.000	0.000
	$H(z) = \frac{0.1}{1-0.9z^{-1}}$	0.019	0.011	0.005	0.019	0.016	0.000	0.005	0.000	0.023	0.028	0.012	0.003	0.006	0.010	0.037	0.038
	$H(z) = \frac{1}{1-0.7z^{-1}}$	0.035	0.049	0.057	0.030	0.056	0.042	0.042	0.056	0.053	0.040	0.050	0.054	0.039	0.062	0.055	0.053

St.: Stationary; N.St.: Non-stationary.

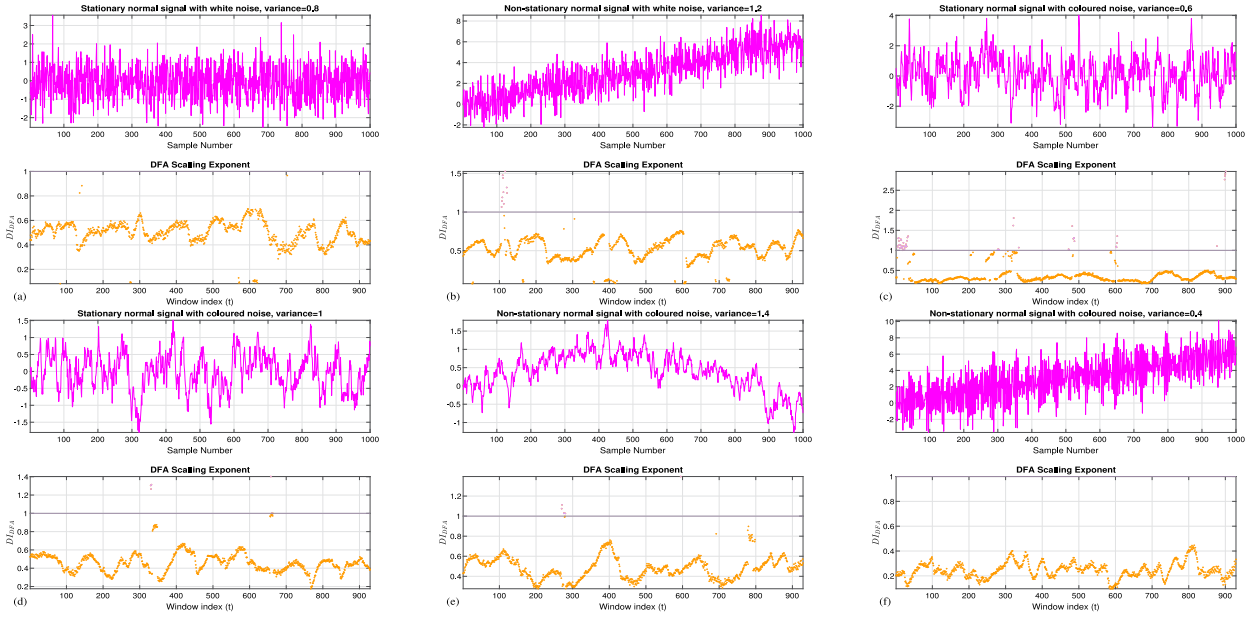

Fig. 4. DI_{DFA} computed using a moving window for several non-oscillatory simulated case studies.

6.1. Non-oscillatory signals

Under the non-oscillatory case studies, the white noise of zero mean and variances varying from 0.2 to 1.6 was incorporated. In contrast, the coloured noise signals were generated by passing the white noise through a filter to eliminate specific frequency components. Using the suggested time scales in Section 4, DI_{DFA} was estimated for each window being analysed. As can be seen from Table 1, the FAR did not exceed 7% i.e., $P_{\text{FA}} < 0.07$ was recorded throughout all case studies. It is noteworthy that increasing the variance does not affect the DI_{DFA} computations. Moreover, the method adopted to compute the DFA, suggested in Hardstone et al. (2012), ensures that the effect of the trend is eliminated, which is readily discernible from the obtained results for the non-stationary case studies. Fig. 4 illustrates the monitoring results of some case studies with different noise scenarios. As shown, DI_{DFA} for the whole signal range remained persistently below the threshold since no oscillations were injected at this stage.

6.2. Multiple oscillations

Signal 1 is a multiple oscillations signal exhibiting two normalised frequencies, 0.1 and 0.3 rad/sample (15 and 45 Hz), contaminated with coloured noise. The online monitoring result is illustrated in Fig. 5 (left); the decision rule based on DI_{DFA} was able to adequately detect the presence of oscillations for the whole signal range starting from the first investigated window without any delay, achieving $P_{\text{FD}} = 1$.

After the detection of the oscillations, IEWT was applied to identify the oscillating components. In this phase, only 200 samples were used in order to illustrate the efficacy of IEWT in extracting the oscillatory modes, even for signals having few cycles. As demonstrated in Fig. 6, the decomposition process reveals that the signal is iteratively decomposed into two components. The power spectrum contains distinct spikes that might be inaccurately extracted as a significant mode, despite stemming from the presence of coloured noise. IEWT captured primarily the mode comprising the highest power in the spectrum, and the corresponding filter was applied to extract the first component in the first stage of Fig. 6. In the second stage, the residual signal was derived, and the corresponding I_{DFA} was computed in order to test if any oscillatory signals were still present in the residual. Subsequently, $I_{DFA} = 1.02258 > 1$ was recorded on the linear part of $\log(v^{(l)}(\Delta))$ versus $\log(\Delta)$; this signifies that the signal needs further decomposition. Hence, the next peak on the power spectrum was identified, and the second component was extracted with the designated filter. By repeating the same procedure, the new residual was computed, and the associated I_{DFA} was found to be $0.058013 \leq 1$, suggesting that no more oscillations can be found in the signal.

To compare the filter bank adopted using EWT and the proposed IEWT, Fig. 7 demonstrates how the power spectrum is split using both methods. Based on the scale-space approach, the boundaries derived using EWT resulted in seven significant regions where even segments representing the noise are kept. This indicates the inability of the conventional EWT to distinguish Fourier supports that are insignificant. The original EWT depends on finding the lowest minimum between

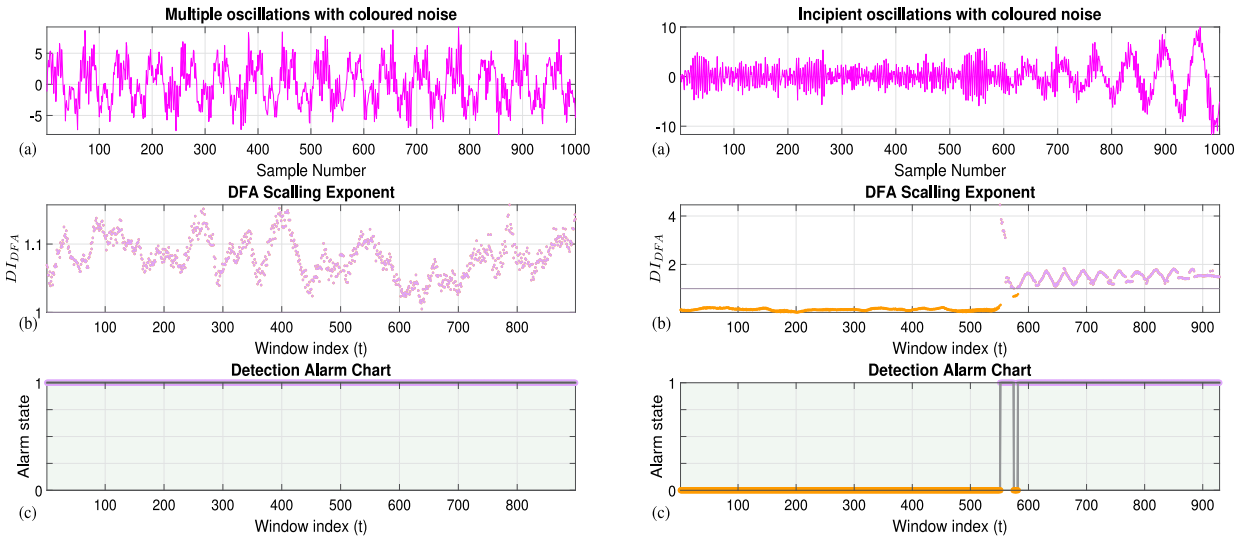

Fig. 5. Multiple oscillations (left) and incipient oscillation (right) online monitoring results of (a) the original signal, (b) its DI_{DFA}, and (c) the detection alarm chart.

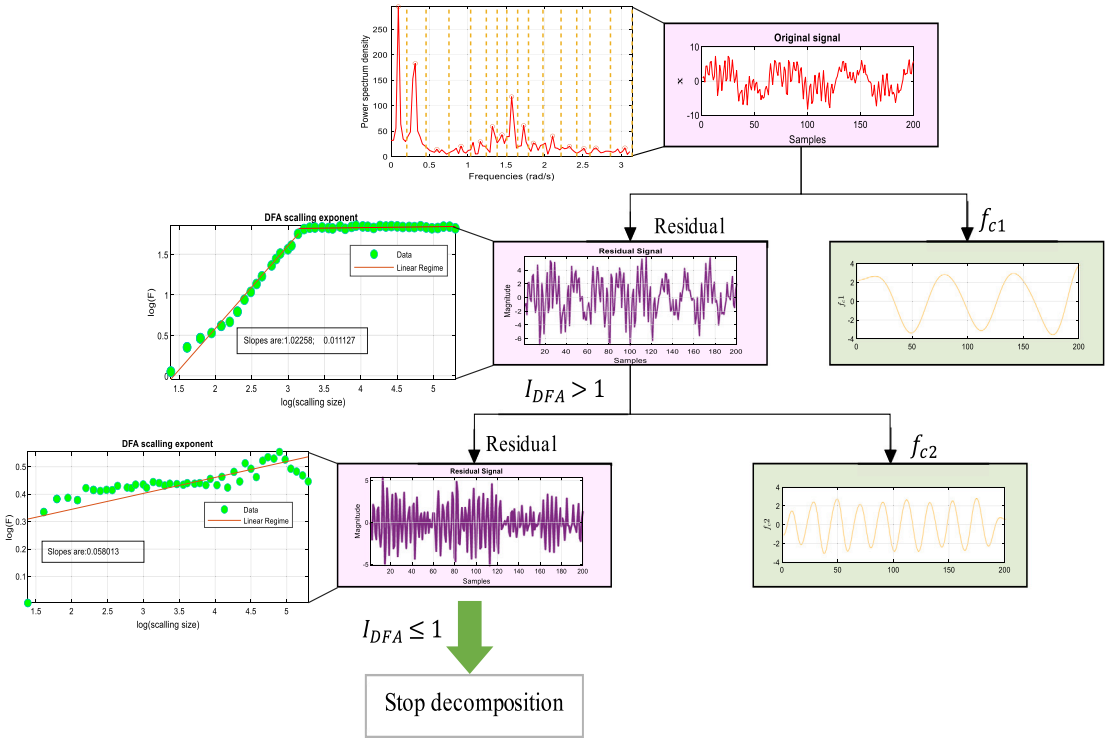

Fig. 6. The proposed IEWT applied to a portion of a signal oscillating at two frequencies corrupted by coloured noise.

consecutive local maxima to split the spectrum; however, this method was proven unrealistic since the number of modes must be known in advance. Therefore, an advanced method was proposed by Gilles and Heal (2014) by creating a scale-space representation of the Fourier spectrum through a convolution of the spectrum with the Gaussian kernel. Then the local minima are detected at each scale to construct a binary scale-space map of minima. The boundaries are then defined by two local minima corresponding to two scale-space curves longer than a certain threshold, where the threshold is computed using Otsu's method, and the filter bank is applied to all segments. This type of segmentation usually results in many inconsistent modes and/or the presence of multiple modes within one segment. This type of segmentation usually results in many inconsistent modes and/or the presence of multiple modes within one segment. On the contrary, the proposed IEWT divided the spectrum into 16 segments; however, the filter bank was only applied to two segments containing the most relevant frequencies by using the potentials of I_{DFA} in determining the oscillating modes, while the segments that do not conform to this rule were discarded as noise. This gives the accurate decomposition where the two components with their frequencies $F\left(f_{c1}\right) = 0.0942$ rad/s and $F\left(f_{c2}\right) = 0.3142$ rad/s which are approximately equal to the true frequencies as shown in Table 2.

6.3. Incipient oscillations

Signal 2 is a case where oscillations were injected slowly at frequency 0.1 rad/sample with coloured noise so that they appear gradually in the time series, as shown in Fig. 5 (right). The oscillations were

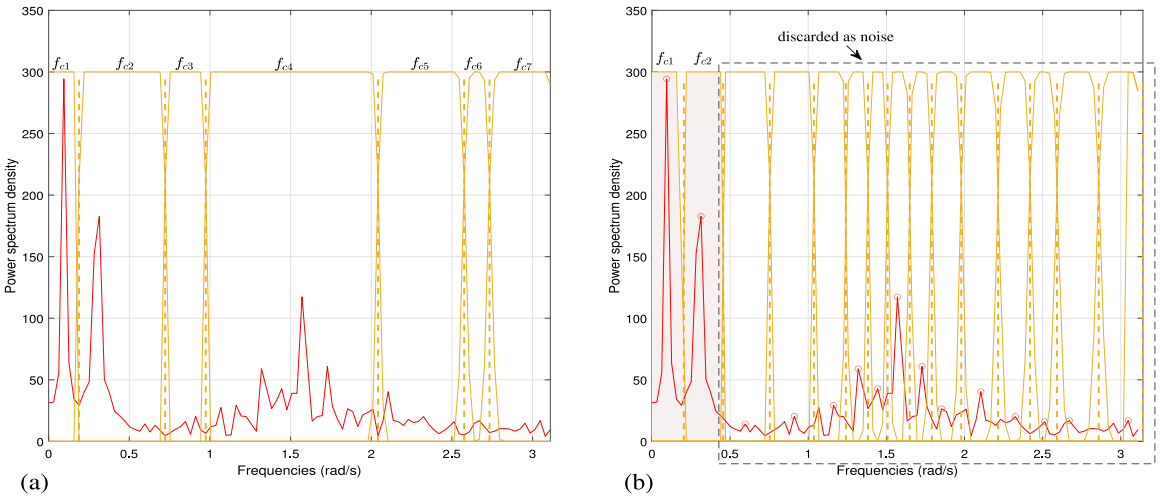

Fig. 7. The filter-bank boundaries on the power spectrum using (a) EWT and (b) IEWT.

Table 2
Monitoring results of the oscillatory simulated case studies.

Data set	Oscillations type	FAR	FDR	TD	Estimated modes	I_{DFA} (residual)	True modes
Sig_1	Multiple	-	1	0	$F(f_{c1}) = 0.0942$ $F(f_{c2}) = 0.3142$	1.0430 0.2168	$F(f_{c1}) = 0.1$ $F(f_{c2}) = 0.3$
Sig_2	Incipient	0	0.9822	20	$F(f_{c1}) = 0.0938$	0.1054	$F(f_{c1}) = 0.1$
Sig_3	Multiple-incipient	0	0.8680	13	$F(f_{c1}) = 0.3751$ $F(f_{c2}) = 0.0938$ $F(f_{c3}) = 0.4689$	1.3110 1.1670 0.1136	$F(f_{c1}) = 0.37$ $F(f_{c2}) = 0.1$ $F(f_{c3}) = 0.46$
Sig_4	Intermittent	0.0129	0.9744	42/29	$F(f_{c1}) : Trend$ $F(f_{c2}) = 0.386$ $F(f_{c3}) = 0.5627$	1.1619 0.5736 0.2782	$F(f_{c1}) : Trend$ $F(f_{c2}) = 0.377$ $F(f_{c3}) = 0.565$
Sig_5	Square	-	1	0	$F(f_{c1}) = 0.0942$ $F(f_{c2}) = 0.3142$ $F(f_{c3}) = 0.5027$ $F(f_{c4}) = 0.6912$ –	1.3817 1.2145 1.0538 0.8184 –	$F(f_{c1}) = 0.1$ $F(f_{c2}) = 0.3$ $F(f_{c3}) = 0.5$ $F(f_{c4}) = 0.7$ $F(f_{c5}) = 0.9$
Sig_6	Non-stationary square	-	1	0	$F(f_{c1}) : Trend$ $F(f_{c2}) = 0.0959$ $F(f_{c3}) = 0.3038$ $F(f_{c4}) = 0.5036$ $F(f_{c5}) = 0.7035$ –	1.6618 1.4131 1.2835 1.2097 0.5283 –	$F(f_{c1}) : Trend$ $F(f_{c2}) = 0.1$ $F(f_{c3}) = 0.3$ $F(f_{c4}) = 0.5$ $F(f_{c5}) = 0.7$ $F(f_{c6}) = 0.9$

$F(f_{ck})$ is the normalised frequency (rad/sample) of the mode f_{ck}.

added at sample 600. The results show the reliable detection of the oscillations, with the first alarm triggered after 20 samples. This TD is interpreted as the window before this instant might contain more data belonging to the normal condition, which dominates over the computations of DI_{DFA}. As illustrated in Table 2, zero false alarms were recorded before the detection time with a detection rate of 98.22% (i.e. $P_{\text{FD}} = 0.9822$ was attained).

The decomposition using EWT is shown in Fig. 8(a), where seven modes were derived. To a certain extent, the first mode represents the true oscillatory mode; however, the mode was slightly noisy due to the involvement of more noise components in the first segment when the power spectrum was divided. Moreover, the six remaining modes that appear to be oscillatory are, in fact, caused by the coloured noise present in the signal. This clearly confirms the deficiency of the standard EWT in extracting spurious modes without any definite criterion specifying which modes to keep. On the other hand, Fig. 8(b) illustrates the proficiency of IEWT in extracting the only oscillatory component present in the signal. After removing this component, I_{DFA} of the residual signal fell below one, and the decomposition was finished. Furthermore, Fig. 8(c) is the decomposition result of the whole range of oscillations, proving that the signal's sample size does not affect the effectiveness of the proposed IEWT method.

To further demonstrate the usefulness of IEWT in accurately extracting the pertinent components, the obtained results are compared to the most used decomposition methods in the literature applied to CPM. The Noise-Assisted EMD (NA-EMD) (Wu and Huang, 2009), ITD (Frei and Osorio, 2007), and VMD (Dragomiretskiy and Zosso, 2014). These techniques were applied to the incipient oscillations in signal 2, and their decomposition results are depicted in Fig. 9. The common problem with these decomposition techniques is the extraction of noisy components, especially with methods that extract high-frequency components first. NA-EMD performed better than ITD and VMD; however, the over-decomposition is still present. Undoubtedly, IEWT outperforms these methods, with the exact extraction of the oscillating mode exhibiting a notable decomposition improvement.

Signal 3 is another case exposing the incipient degradation but with noise-contaminated multiple oscillations, namely, at 0.1, 0.37, and 0.46 rad/sample. In this case, the first alarm was triggered after the degradation was injected by 13 samples, resulting in zero FAR and 86.8% FDR. DFA-based online monitoring was effective in detecting such small drifts and recognising single and multiple oscillations with slight TD as shown in Fig. 10(left). IEWT was successful in extracting the modes where a sequence of $I_{DFA} = \{1.3110; 1.2097; 0.5283\}$ of

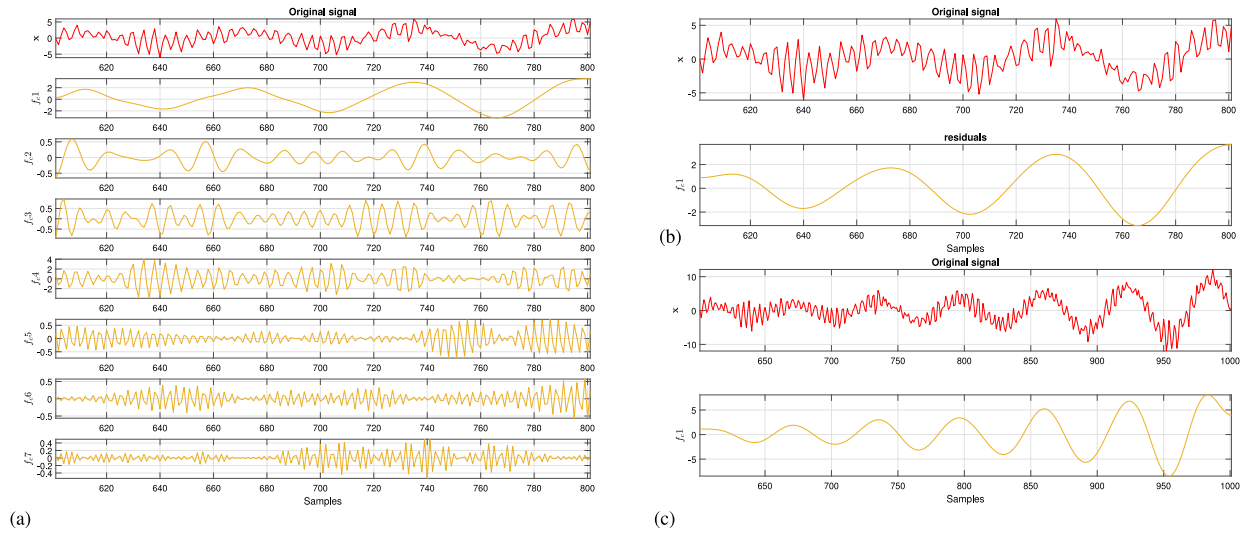

Fig. 8. Decomposition results of the incipient oscillations using (a) EWT and (b) IEWT at the earliest stage, and (c) using IEWT for the whole oscillating range.

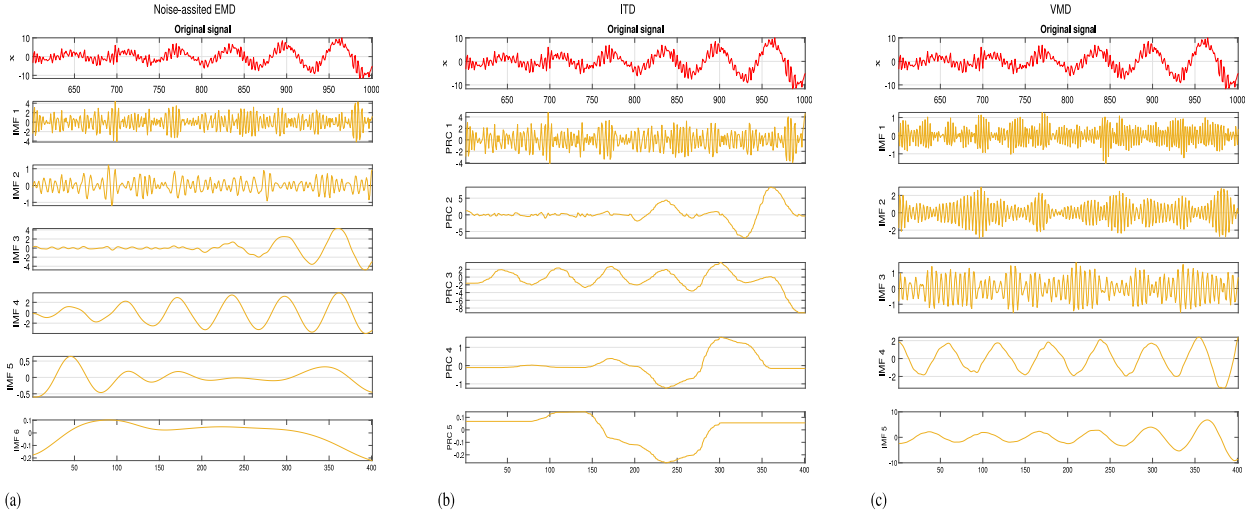

Fig. 9. Decomposition results of the incipient oscillations using (a) NA-EMD, (b) ITD, and (c) VMD for the whole oscillating range.

the residuals was obtained to stop the decomposition, resulting in the correct three modes as shown in Table 2 and Fig. 11(a). I_{DFA} decreased when the second component was extracted from its initial value after subtracting the first component since the data contains a high noise level. Nevertheless, I_{DFA} was still greater than one, implying that oscillations are still present in the signal. Obtaining $I_{DFA} = 0.5283$ at the last stage indicates precisely that the residual is purely noisy without any oscillations. Fig. 12 demonstrates further the deficiency of the existing methods in dealing with noisy oscillating signals.

6.4. Intermittent oscillations

Signal 4 exemplifies the intermittent oscillations case study where oscillations are introduced between 100 to 300 samples at 0.377 rad/sample and 700 to 1000 samples at 0.565 rad/sample with a white noise of zero mean and 0.6 variance. Again, DFA accomplished satisfactory monitoring results as shown in Fig. 10(right) given the high level of noise incorporated (97.44% FDR after fault detected within 42 and 29 samples from the occurrence of the first oscillatory interval and second, respectively and with 1.29% FAR in portions without degradation).

IEWT was implemented only on the time series where oscillations were detected and could accurately extract the modes existing in the two intervals (see Fig. 11(b and c) and Table 2). This illustrates the advantage of combining the online detection using DFA with a decomposition method where only intervals exhibiting oscillations are decomposed to identify the characteristics of the degradation without the need to decompose even normal signals.

6.5. Square oscillations

Square waves are a common type of nonlinear oscillation encountered in faulty control loops. Therefore, two case studies (signal 5 and 6 with non-stationarity) were tested using the DFA-IEWT framework to demonstrate its efficacy in the simultaneous extraction of non-stationarities and nonlinearities. The results, depicted in Fig. 13, show that these oscillations were amply detected with 100% FDR in the online monitoring phase, where the trend in signal 6 did not affect the efficiency of DFA. Furthermore, these signals are composed of one fundamental frequency at 0.1 rad/sample and odd harmonics at 0.3; 0.5; 0.7; 0.9 rad/sample. Employing both EWT and IEWT on signals proves the deficiency of EWT in segmenting the power spectrum properly (see Fig. 14), resulting in erroneous decomposition as shown in Fig. 15(a). The same problem was encountered with NA-EMD and ITD as shown in Fig. 16; although, VMD performed better this time

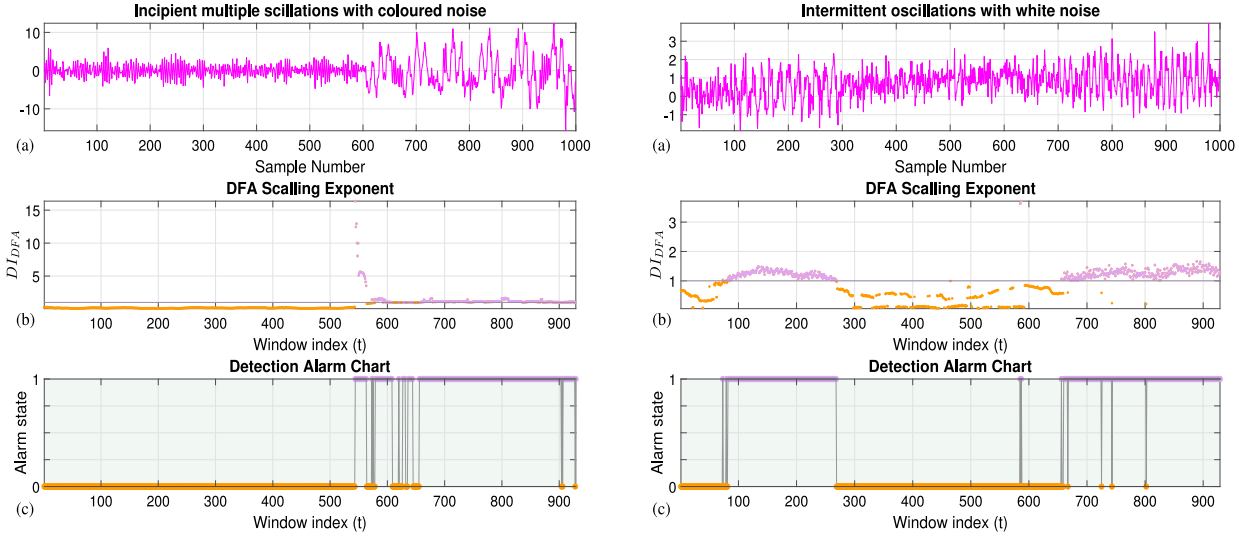

Fig. 10. Incipient multiple oscillations (left) and intermittent oscillations (right) online monitoring results of (a) the original signal, (b) its DI_{DFA}, and (c) the detection alarm chart.

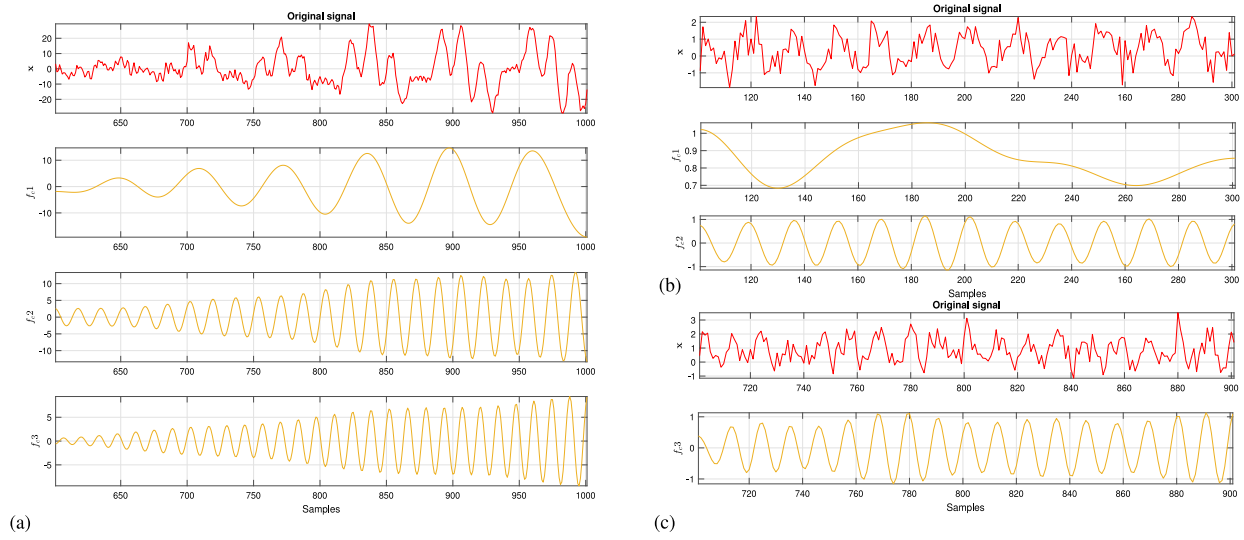

Fig. 11. Decomposition results using IEWT on (a) Sig_3 (incipient multiple oscillations) and Sig_4 (b) the first portion of the intermittent oscillations and (c) the second portion.

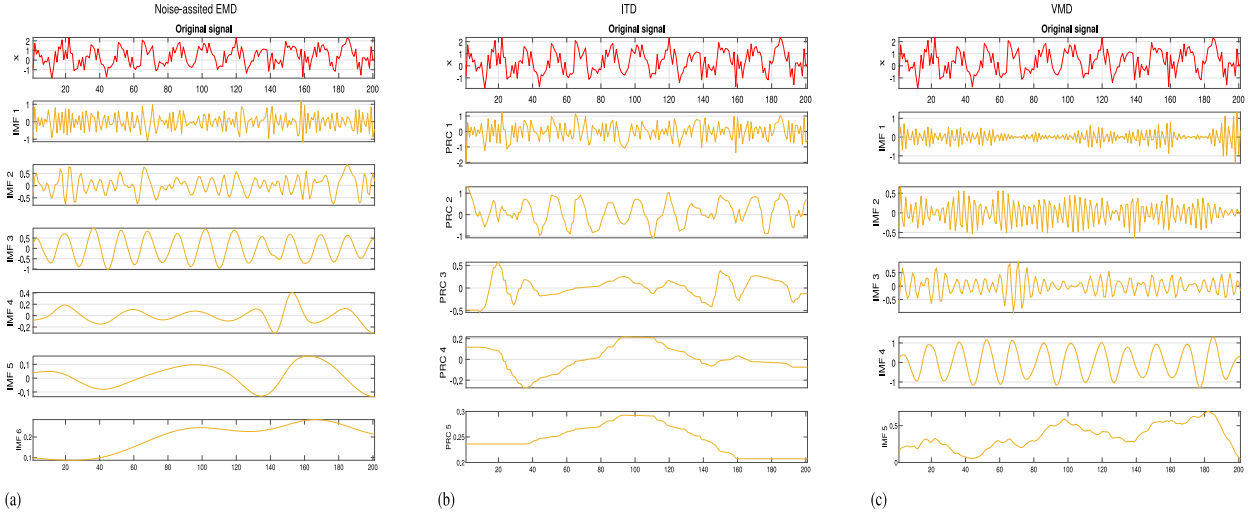

Fig. 12. Decomposition results of the first portion of the intermittent oscillations Sig_4 using (a) noise-assisted EMD, (b) ITD, and (c) VMD.

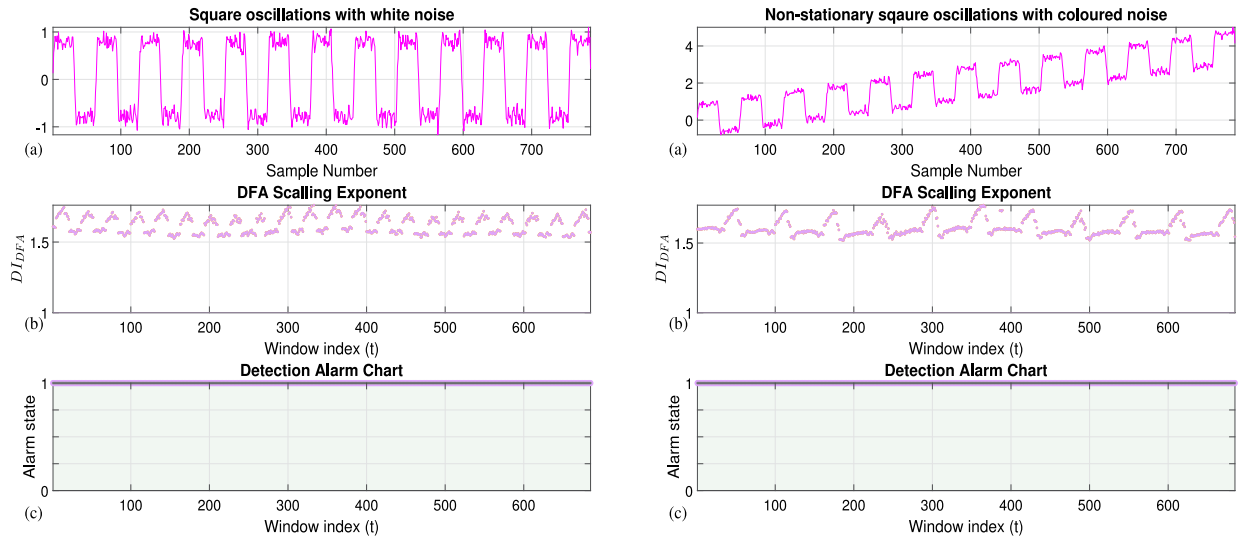

Fig. 13. Square-wave oscillations (left) and the non-stationary square-wave oscillations (right) online monitoring results of (a) the original signal, (b) its DI_{DFA}, and (c) the detection alarm chart.

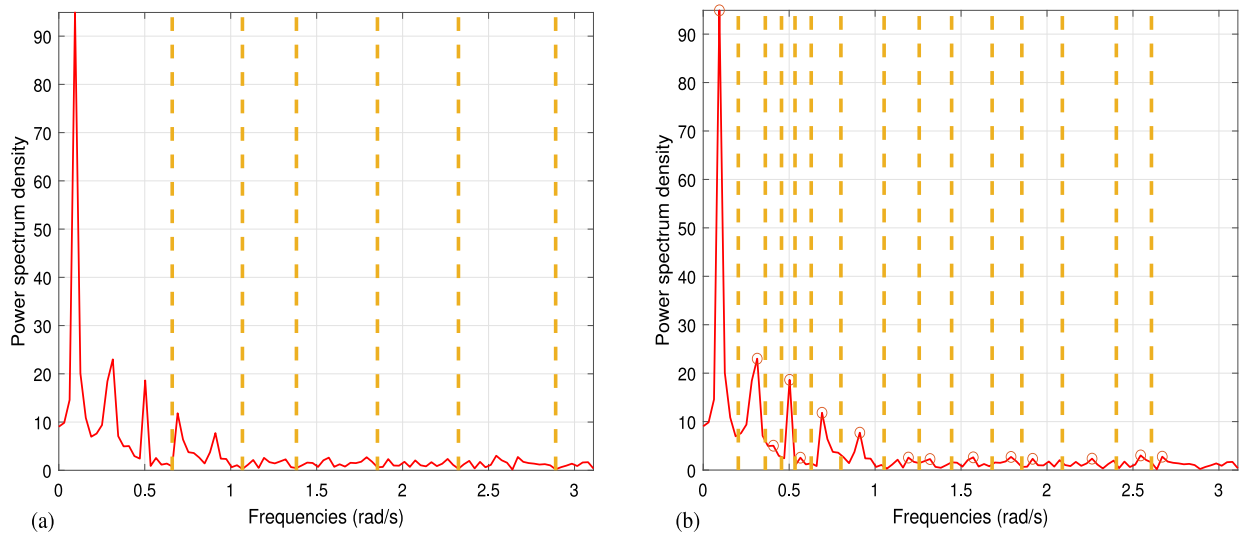

Fig. 14. The filter-bank boundaries on the power spectrum using (a) EWT and (b) IEWT.

which illustrates that these methods cannot be generalised to all the types of oscillations. In contrast, the proposed IEWT was capable of precisely extracting the components up to the 7th harmonic. For signal 6, the trend was additionally correctly identified, which represents the component extracted at zero frequency for both small sample size and by considering the whole signal range (Fig. 17).

6.6. Computational costs

The run time is evaluated in this work by increasing the sample size of the time series. Table 3 displays the computational time in seconds. The algorithms were executed on a computer equipped with an Intel(R) Core(TM) i5-10210U CPU @ 1.60 GHz with 16 GB RAM. Since the proposed algorithm consists of two stages where the malfunctions are detected in real time at the first stage by considering the sliding window mode, the time complexity grows with an increase in sample size. However, considering its remarkable performance, analysing a single window merely takes 0.201 s. The decomposition approaches that have been compared in this work tend to decompose the signals in an offline mode which is comparable to the second stage of the proposed algorithm, IEWT. As can be seen from the table, the computing expenses of all the algorithms are roughly the same. ITD and VMD have the lowest computational costs among the methods, however, with poor decomposition performance. Moreover, the proposed IEWT requires less run time for larger sample sizes than EWT and NA-EMD with a significantly higher level of accuracy in identifying the exact oscillating modes.

7. Case study 2: Industrial application

In a further step towards corroborating the proficiency of the proposed DFA-IEWT online monitoring methodology, 11 case studies were selected from the publicly available data repository offered by Jelali and Huang (Jelali and Huang, 2021, 2010). These involve data from healthy as well as oscillating control loops derived from diverse industries, including metal, buildings, power, chemical, and pulp and paper. The input to the monitoring system is chosen either as the Process Variable (PV) or the controller Output (OP).

7.1. Non-oscillatory loops

This represents the non-oscillating time series gathered from four control loops: 1 gauge, two temperature, and 1 level control loops.

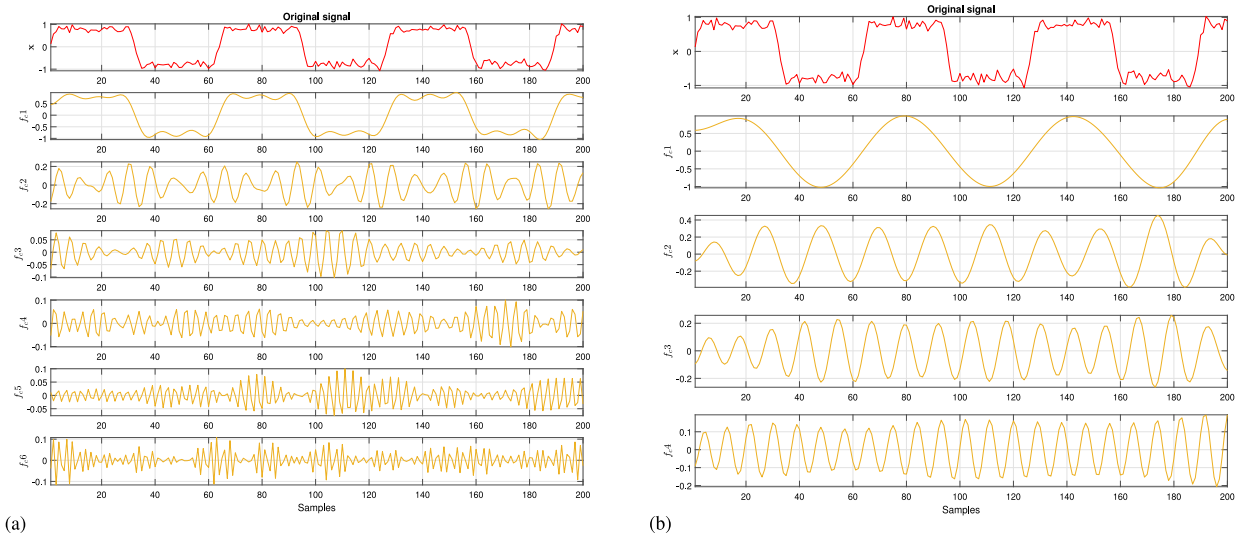

Fig. 15. Decomposition results of square-wave oscillations using (a) EWT and (b) IEWT.

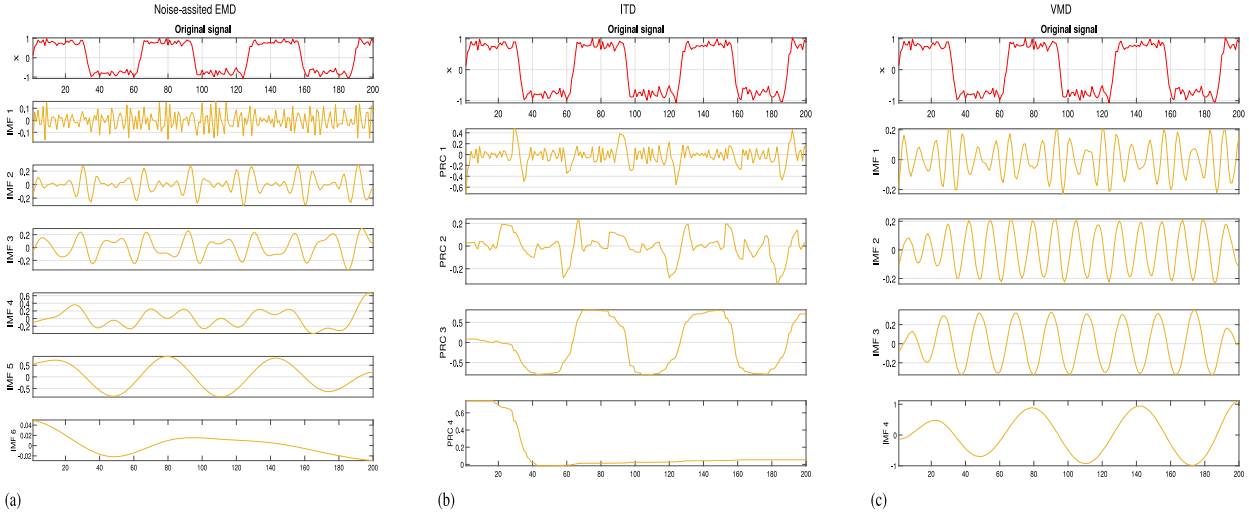

Fig. 16. Decomposition results of the square wave Sig_5 using (a) noise-assisted EMD, (b) ITD, and (c) VMD.

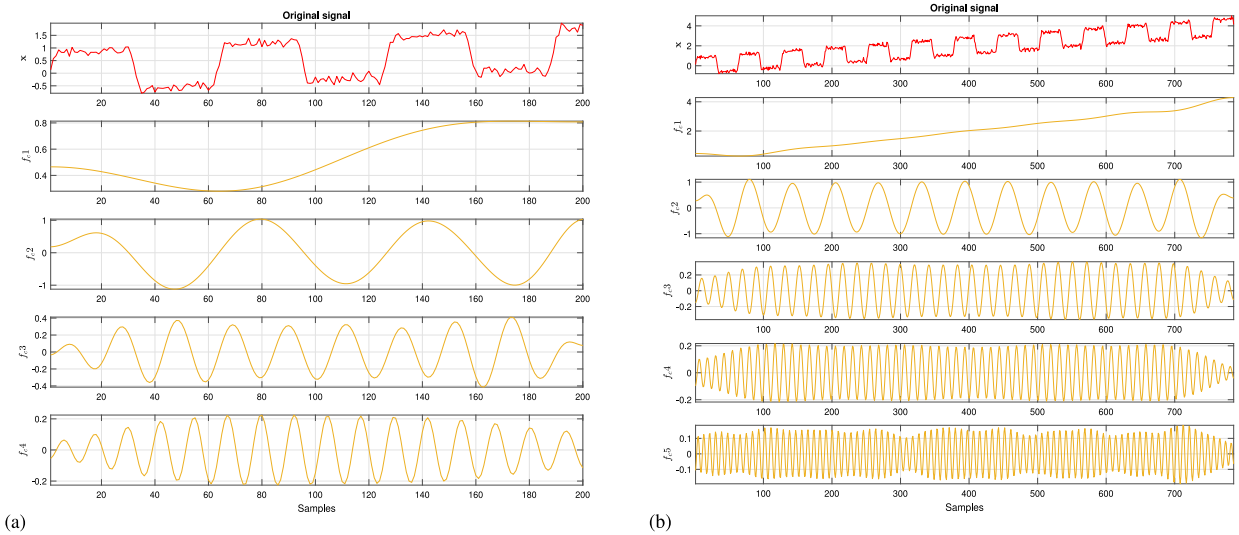

Fig. 17. Decomposition results using IEWT on the non-stationary square wave Sig_6 (a) a small sample size and (b) the whole signal.

Table 3
Comparison of the computational time in terms of the number of samples processed.

Samples	Method					
	DFA	IEWT	EWT	NA-EMD	ITD	VMD
100	4.182 s	2.576 s	2.200 s	5.037 s	1.717 s	1.899 s
500	30.219 s	3.701 s	2.647 s	9.025 s	2.006 s	2.277 s
1000	65.038 s	5.903 s	4.175 s	11.979 s	2.096 s	2.214 s
5000	356.065 s	11.743 s	33.220 s	37.220 s	1.987 s	2.720 s

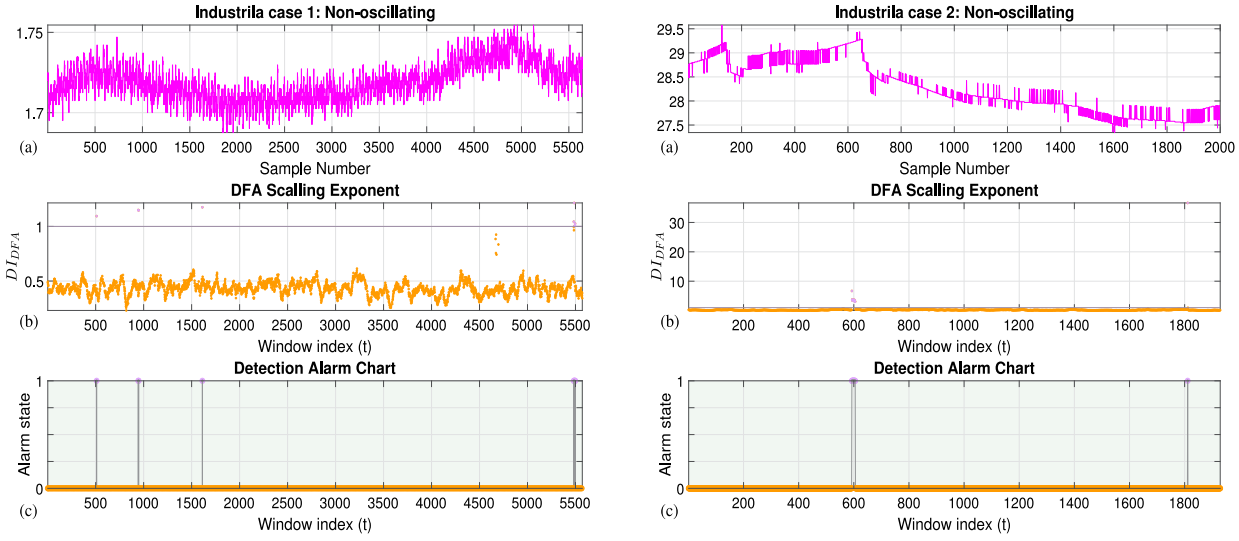

Fig. 18. The non-oscillatory industrial case 1 (left) and 2 (right) online monitoring results of (a) the original signal, (b) its DI_{DFA}, and (c) the detection alarm chart.

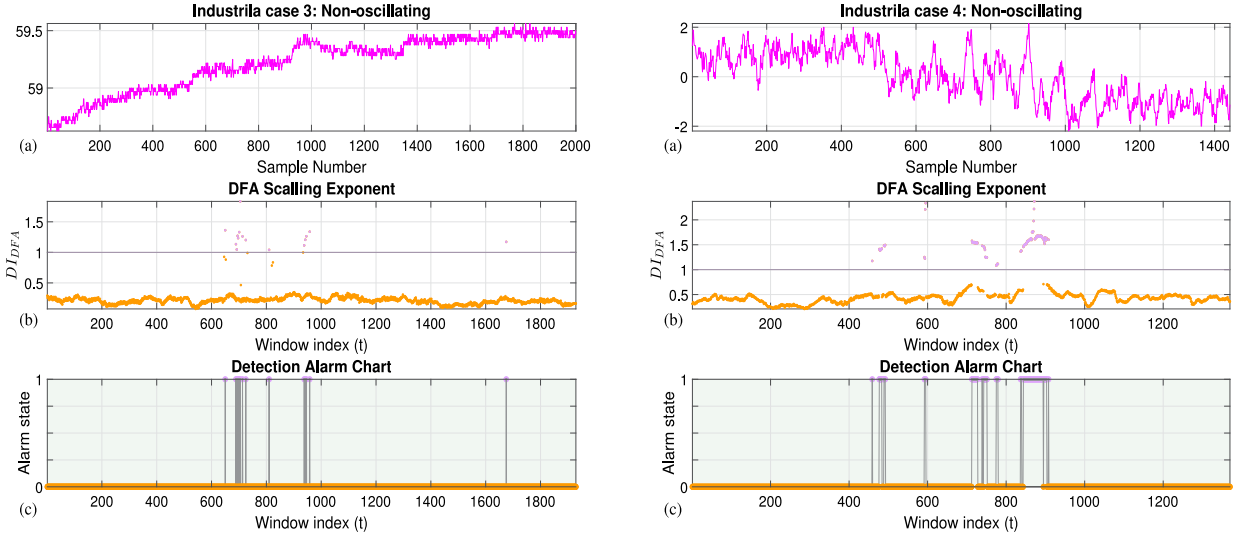

Fig. 19. The non-oscillatory industrial case 3 (left) and case 4 (right) online monitoring results of (a) the original signal, (b) its DI_{DFA}, and (c) the detection alarm chart.

The real-time monitoring results are shown in Figs. 18 and 19. During the online detection procedure, DI_{DFA} remained below the threshold for practically every temporal frame; therefore, the signals were successfully assigned as non-oscillating. The obtained FAR was relatively negligible as it did not exceed 8% for all case studies (the individual results are shown in Table 4). As a result, since no oscillations were detected, it is no longer necessary to proceed to the second stage, which is the decomposition using IEWT.

7.2. Tuning problems

In this case, two signals from level control in a chemical process (case 5) and pulp and paper process (case 11) are evaluated. These two loops are known to oscillate due to bad tuning. The oscillations for both cases were accurately detected using DI_{DFA}, reaching a 100% detection rate and a zero delay. The oscillations necessitated the application of IEWT to derive their characteristics. As shown in Figs. 20(left) and 21(b) and Table 4, the signal from case 5 is clearly non-stationary with a trend which was extracted using IEWT along with the main oscillating mode $F\left(f_{c1}\right) = 0.3770$. However, EWT over-decomposed the signal to many unrealistic modes that emerged due the presence of noise. The decomposition of this signal was also explored using NA-EMD, ITD, and VMD as shown in Fig. 22. Clearly, these three methods failed to identify the important modes where they indicated the presence of multiple oscillations. In contrast, a single mode $F\left(f_{c1}\right) = 0.0452$ was

Table 4
Monitoring results of the industrial case studies.

Industry	Data set	Loop type	Fault type	FAR	FDR	Modes[a]	Oscillations?
Metal	Ind_1	Gauge	Normal	0.0016	–	–	No
Buildings	Ind_2	Temp.	Normal	0.0070	–	–	No
	Ind_3	Temp.	Normal	0.0075	–	–	No
Chemical	Ind_4	Level	Normal	0.0796	-	–	No
	Ind_5	Level	Tuning problem	-	1.00	$F(f_{c1}) = 0.3770$ $F(f_{c2}) : Trend$	Yes
	Ind_6	Flow	Faulty stream sensor	-	1.00	$F(f_{c1}) : Trend$ $F(f_{c2}) = 0.2513$ $F(f_{c3}) = 0.5341$	Yes
	Ind_7	Level	Disturbance	–	0.8540	$F(f_{c1}) : Trend$ $F(f_{c2}) = 0.1257$	Yes
	Ind_8	Level	Stiction	–	1.00	$F(f_{c1}) = 0.0668$ $F(f_{c2}) = 0.2042$ $F(f_{c3}) = 0.3534$	Yes
	Ind_9	Flow	Stiction	–	0.9706	$F(f_{c1}) : Trend$ $F(f_{c2}) = 0.0483$ $F(f_{c3}) = 0.1449$	Yes
	Ind_10	Flow	Likely disturbance	–	0.9769	$F(f_{c1}) : Trend$ $F(f_{c2}) = 0.7539$ $F(f_{c3}) = 0.5027$	Yes
	Ind_11	Level	Likely disturbance	–	1.00	$F(f_{c1}) : Trend$ $F(f_{c2}) = 0.3770$	Yes
Power	Ind_12	Level	Stiction	–	0.9479	$F(f_{c1}) = 0.1257$ $F(f_{c2}) = 0.2827$ $F(f_{c3}) : Trend$ $F(f_{c4}) = 0.3770$	Yes
	Ind_13	Level	Stiction	-	1.00	$F(f_{c1}) = 0.2813$ $F(f_{c2}) = 0.5626$	Yes
	Ind_14	Level	Stiction	-	1.00	$F(f_{c1}) : Trend$ $F(f_{c2}) = 0.1256$ $F(f_{c3}) = 0.2827$	Yes
Pulp and papers	Ind_15	Level	Tuning problem	–	1.00	$F(f_{c1}) = 0.0452$	Yes
	Ind_16	Flow	Stiction	-	0.8209	$F(f_{c1}) = 0.0353$ $F(f_{c2}) = 0.1276$ $F(f_{c3}) = 0.2513$ $F(f_{c4}) = 0.3907$ $F(f_{c5}) = 0.5301$	Yes
	Ind_17	Conc.	Stiction	-	1.00	$F(f_{c1}) = 0.061$ $F(f_{c2}) = 0.1865$ $F(f_{c3}) = 0.3220$ $F(f_{c4}) = 0.4614$ $F(f_{c5}) = 0.5832$ $F(f_{c6}) = 0.7069$	Yes
	Ind_18	Level	Stiction	–	1.00	$F(f_{c1}) : Trend$ $F(f_{c2}) = 0.2513$ $F(f_{c3}) = 0.1257$ $F(f_{c4}) = 0.5341$ $F(f_{c5}) = 0.6912$	Yes

Temp.: temperature control; Conc.: concentration control.
[a] $F(f_{ck})$ is the normalised frequency (rad/sample) of the mode f_{ck}.

revealed using IEWT for the signal from case 11. The obtained results are consistent with the fact that these signals are undergoing a tuning problem which is a linear abnormality where it is acknowledged that only non-linear faults result in a harmonic oscillation.

7.3. Sensor faults and external disturbances

The suggested method was also put to test a malfunctioning stream sensor from a chemical factory. The loop oscillates and incorporates a trend, as shown in Fig. 20 (right). An FDR of 100% was reached, indicating that the loop is deteriorating. The oscillating modes was derived at two frequencies: $F(f_{c2}) = 0.2513$ and $F(f_{c3}) = 0.5341$, where the trend was also extracted at zero frequency as illustrated in Table 4 and Fig. 23(b). This decomposition outperformed EWT again that resulted in an inaccurate decomposition, as seen in Fig. 23(a). Fig. 24 illustrates the decomposition of this signal using NA-EMD, ITD, and VMD. These techniques typically extract the noise-related components first. Moreover, the oscillatory components were undetectable by NA-EMD and ITD.

Three cases undergoing external disturbance were chosen from level and flow control loops. The disturbances were effectively recognised with an average of 94.36% FDR and applying IEWT led to an explicit decomposition of all the cases where no inconsistent components were extracted (see Table 4).

7.4. Valve stiction

Stiction is the most severe fault encountered in industrial control loops. Five case studies from various industrial facilities were utilised to demonstrate the capabilities of the proposed DFA-IEWT monitoring system in coping with nonlinearities. The results obtained on cases 8, 9, 12, 13, 14, 16, 17, and 18, as summarised in Table 4, yield an average of 96.74% detection rate during the real-time monitoring, which is

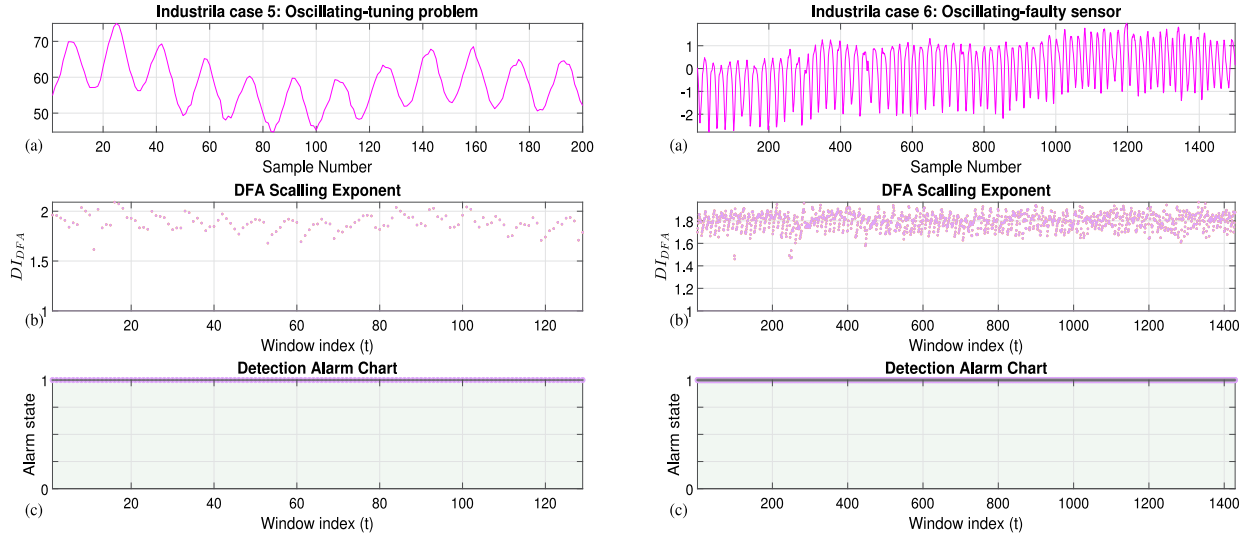

Fig. 20. The oscillating due to a tuning problem industrial case 5 (left) and case 6 (right) oscillating due to a faulty sensor online monitoring results of (a) the original signal, (b) its DI_{DFA}, and (c) the detection alarm chart.

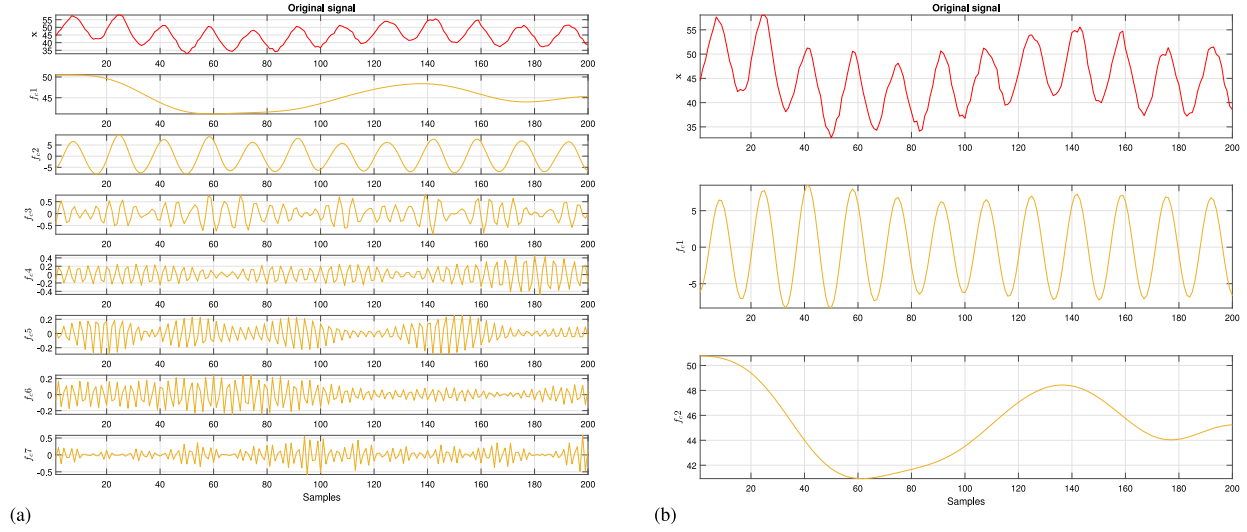

Fig. 21. Decomposition results of industrial case 5 using (a) EWT and (b) IEWT.

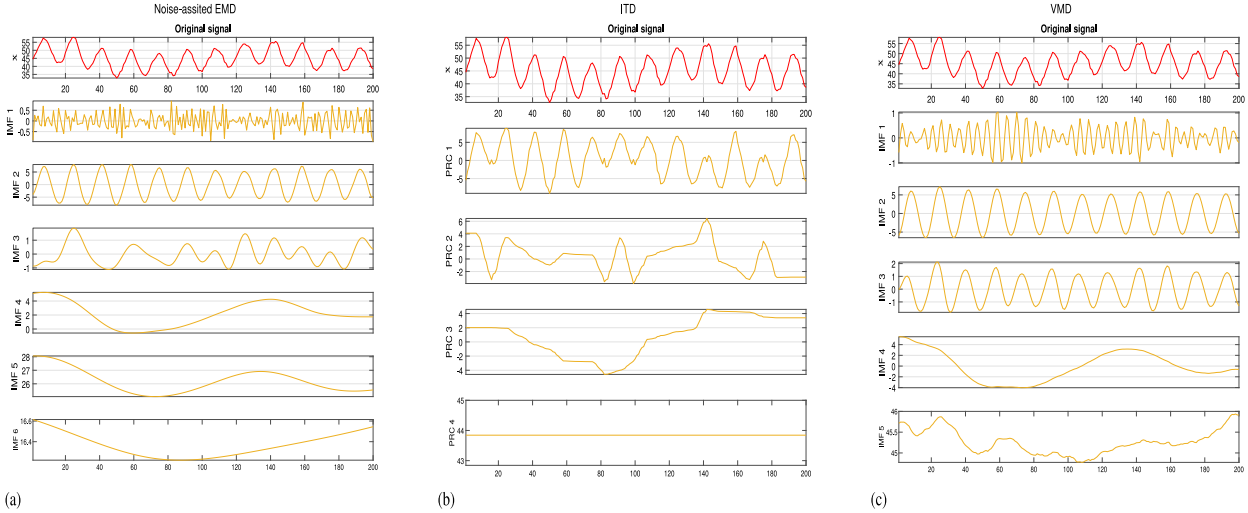

Fig. 22. Decomposition results of industrial case 5 using (a) noise-assisted EMD, (b) ITD, and (c) VMD.

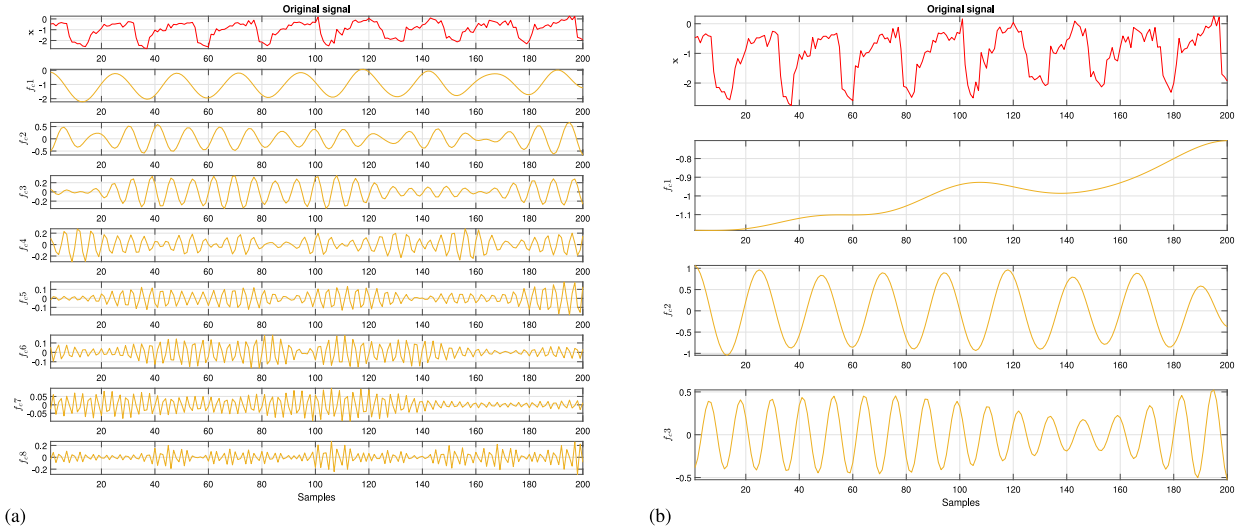

Fig. 23. Decomposition results of industrial case 6 using (a) EWT and (b) IEWT.

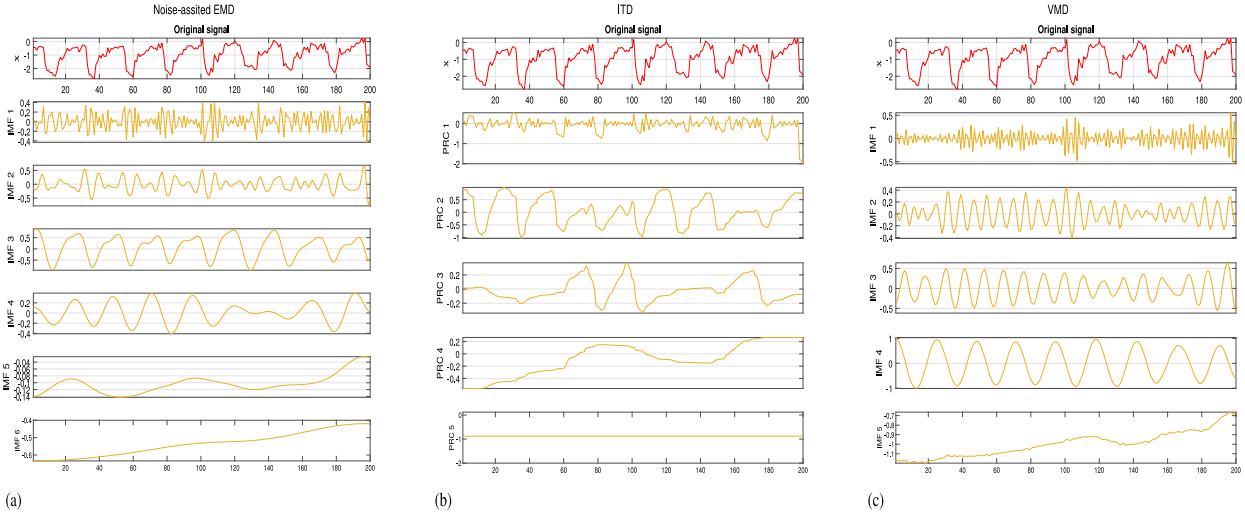

Fig. 24. Decomposition results of industrial case 6 using (a) noise-assisted EMD, (b) ITD, and (c) VMD.

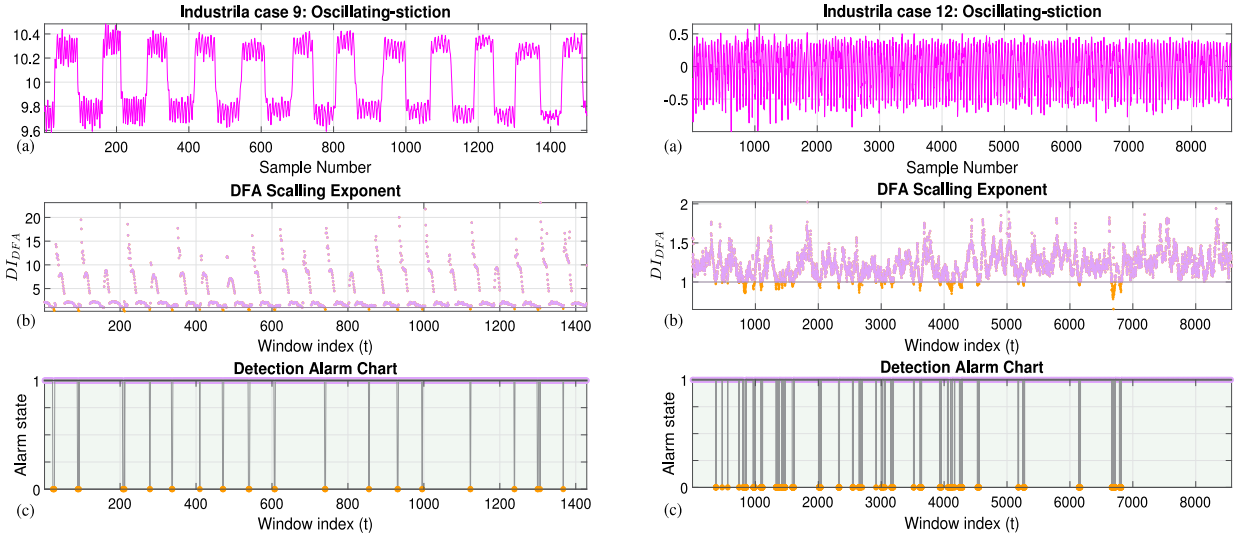

Fig. 25. The oscillating due to stiction industrial case 9 (left) and case 12 (right) online monitoring results of (a) the original signal, (b) its DI_{DFA}, and (c) the detection alarm chart.

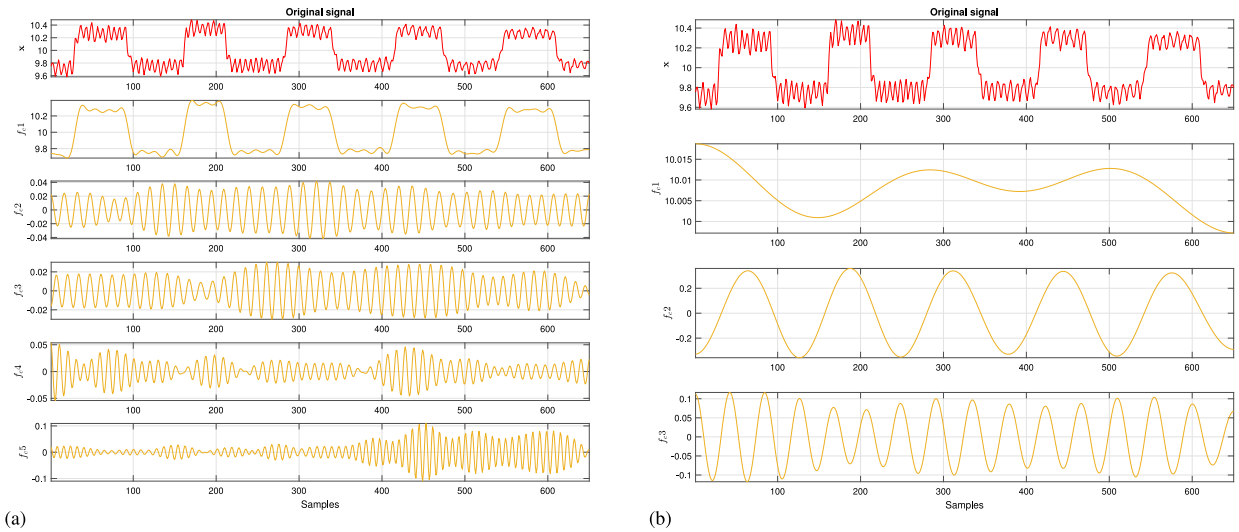

Fig. 26. Decomposition results of industrial case 9 using (a) EWT and (b) IEWT.

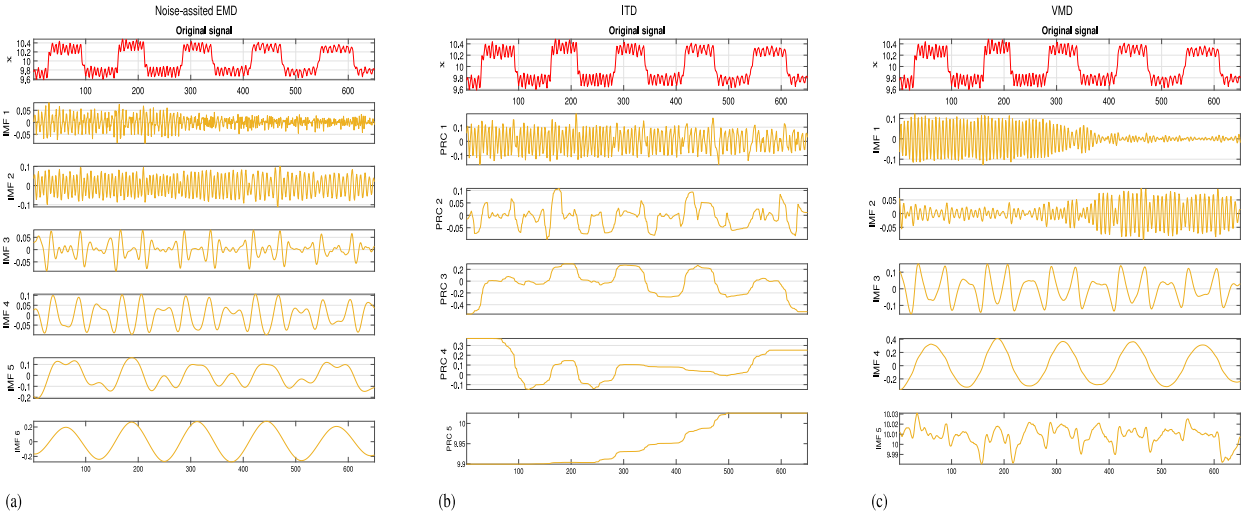

Fig. 27. Decomposition results of industrial case 9 using (a) noise-assisted EMD, (b) ITD, and (c) VMD.

remarkable given the existence of noisy multiple oscillations simultaneously. The monitoring results for cases 9 and 12 are displayed in Fig. 25 while their corresponding decomposition is shown in Figs. 26 and 28, respectively. The decomposition supports the inclusion of harmonics for all the examples and confirms the presence of nonlinearities. By comparison, the decomposition of case 9 produced the same findings as the approach presented by Chen et al. (2020a) using FACMD; however, IEWT demonstrated a better decomposition in recovering even the signal's trend. The decomposition of these signals was also performed using NA-EMD, ITD, VMD as shown in Figs. 27 and 29 where these methods poorly decomposed the signals, especially in the case of noisy squared oscillations.

8. Conclusion

This paper explored the online controller performance monitoring of industrial control loops by utilising a novel suggested technique that combined DFA and EWT. This suggested monitoring system was created in a hierarchical structure to achieve the intended requirements of establishing a CPM system that can function efficiently in real-time while managing the various signal characteristics encountered in practice. In that vein, the basic level detection system identifies deterioration using a new control chart called DI_{DFA} and a complementary level that exposes the patterns of oscillations detected in the first level using the improved EWT. It was demonstrated through the implementations that the assumption-free correlation measure DFA is capable of expressing short- and long-term correlations in time series. Additionally, owing to the findings in the first stage, EWT was improved by incorporating DFA to enhance the decomposition process. IEWT outperformed the conventional EWT and overcame its shortcomings associated with the over-decomposition problem and the erroneous division of the power spectrum. Consequently, the complete DFA-IEWT framework showed satisfactory results in detecting deterioration in an online mode and extracting the oscillatory modes along with their frequencies. This was verified using a considerable number and variety of simulated signals subjected to different normal as well as oscillatory conditions. Non-stationarity and incipient oscillations are two infrequently addressed issues by earlier works in the literature, despite being highly prevalent problems in practical applications. However, the present framework was proficient in dealing with this severe behaviour while requiring no assumptions regarding the time series under consideration. The capabilities of the proposed methodology were further confirmed through an application on a wide range of realistic industrial case studies. Nevertheless, DI_{DFA} may give rise to some undesirable false alarms when the normal testing data appears to possess some oscillatory

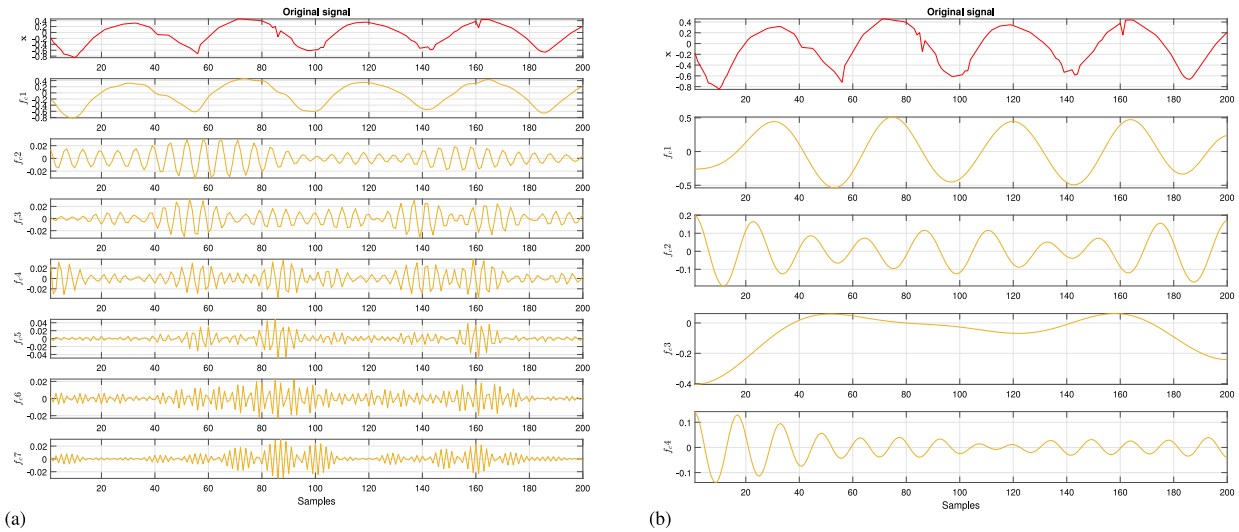

Fig. 28. Decomposition results of industrial case 12 using (a) EWT and (b) IEWT.

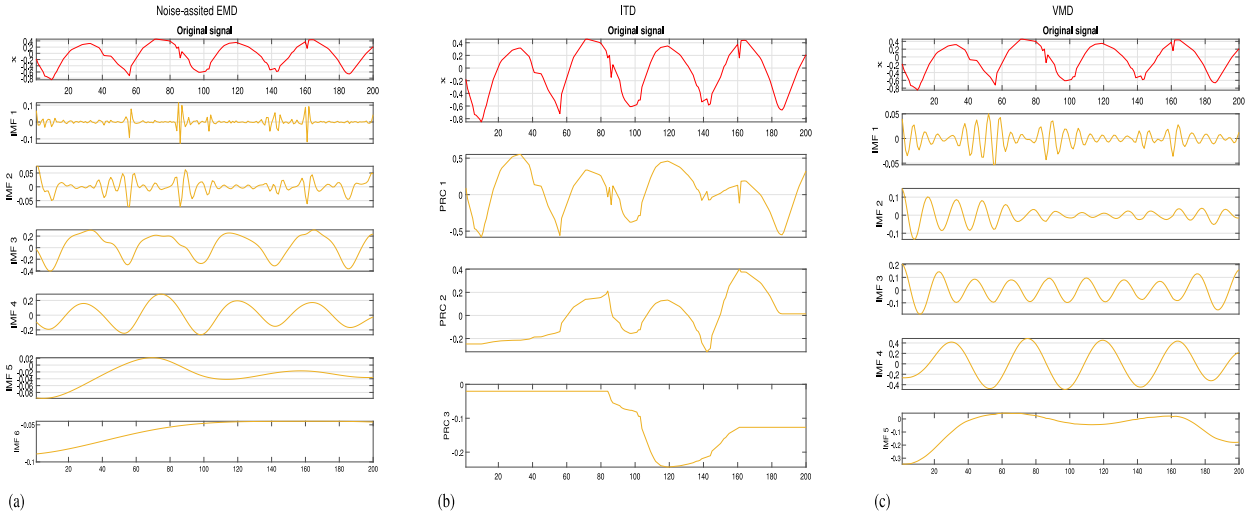

Fig. 29. Decomposition results of industrial case 12 using (a) noise-assisted EMD, (b) ITD, and (c) VMD.

behaviour. Similarly, missed detected instances in faulty cases could also be generated if the noise becomes dominant within the temporal frame when evaluating the statistical index. Ultimately, the presented technique comprehensively addressed deterioration detection in industrial control loops, achieving high accuracy in identifying oscillations in real-time and extracting their characteristic features, which may be helpful for the diagnosis stage in the future. Therefore, the suggested framework offers the following advantages over the methodologies currently employed in the literature:

i. DI_{DFA} provides a purely data-driven means of detecting abnormalities in control loop in real time as soon as a new observation emerges without any adaptability of parameters.
ii. DI_{DFA} is a nonlinear measure with the ability to take into account the systems' dynamics and identify nonlinear correlations.
iii. This method is robust to both white and coloured noise while most of the existing methods fails to deal with coloured noise.
iv. All forms of anomalies, including incipient, intermittent, and multiple oscillations, can be handled by this technique, which offers an assumption-free system for monitoring controller performance.
v. The improved EWT (IEWT) decomposition technique is applied only if the loop is confirmed to be oscillating.
vi. A new stopping criterion was established to cope with the overdecomposition problem encountered in all the decomposition techniques compared in this work.
vii. The capacity of IEWT to extract only the important oscillation modes eliminates any potential for uncertainty.

CRediT authorship contribution statement

Wahiba Bounoua: Conceptualization, Formal analysis, Investigation, Methodology, Software, Validation, Visualization, Writing – original draft, Writing – review & editing. **Muhammad Faisal Aftab:** Conceptualization, Supervision, Resources, Writing – review & editing. **Christian Walter Peter Omlin:** Conceptualization, Supervision, Resources, Writing – review & editing.

Declaration of competing interest

The authors declare that they have no known competing financial interests or personal relationships that could have appeared to influence the work reported in this paper.

Data availability

The data is available online.

References

Aftab, M.F., Hovd, M., Sivalingam, S., 2018. Improved oscillation detection via noise-assisted data analysis. Control Eng. Pract. 81, 162–171. http://dx.doi.org/10.1016/j.conengprac.2018.08.019, URL https://linkinghub.elsevier.com/retrieve/pii/S0967066118304726.

Ahad, M.A.R., Ahmed, M.U. (Eds.), 2021. Signal Processing Techniques for Computational Health Informatics. In: Intelligent Systems Reference Library, vol. 192, Springer International Publishing, Cham, http://dx.doi.org/10.1007/978-3-030-54932-9, URL https://link.springer.com/10.1007/978-3-030-54932-9.

Aldrich, C., Auret, L., 2013. Unsupervised Process Monitoring and Fault Diagnosis with Machine Learning Methods. Springer London, London, http://dx.doi.org/10.1007/978-1-4471-5185-2, URL http://link.springer.com/10.1007/978-1-4471-5185-2.

Amezquita-Sanchez, J.P., Adeli, H., 2015. A new music-empirical wavelet transform methodology for time–frequency analysis of noisy nonlinear and non-stationary signals. Digit. Signal Process. 45, 55–68. http://dx.doi.org/10.1016/j.dsp.2015.06.013, URL https://linkinghub.elsevier.com/retrieve/pii/S1051200415001992.

Amin, M.T., Khan, F., 2022. Risk assessment in Industry 4.0. In: Methods in Chemical Process Safety. Vol. 6. Elsevier, pp. 631–651. http://dx.doi.org/10.1016/bs.mcps.2022.05.003, URL https://linkinghub.elsevier.com/retrieve/pii/S2468651422000137.

Bounoua, W., Aftab, M.F., Omlin, C.W.P., 2022. Controller performance monitoring: A survey of problems and a review of approaches from a data-driven perspective with a focus on oscillations detection and diagnosis. Ind. Eng. Chem. Res. 61 (49), 17735–17765. http://dx.doi.org/10.1021/acs.iecr.2c02785, URL https://pubs.acs.org/doi/10.1021/acs.iecr.2c02785.

Chandrasekhar, E., Dimri, V.P., Gadre, V.M. (Eds.), 2013. Wavelets and Fractals in Earth System Sciences. CRC Press, http://dx.doi.org/10.1201/b16046, URL https://www.taylorfrancis.com/books/9781466553606.

Chau, K., Djire, A., Vaddiraju, S., Khan, F., 2022. Process Risk Index (PRI) – A methodology to analyze the design and operational hazards in the processing facility. Process Saf. Environ. Prot. 165, 623–632. http://dx.doi.org/10.1016/j.psep.2022.07.049, URL https://linkinghub.elsevier.com/retrieve/pii/S0957582022006619.

Chen, Q., Chen, J., Lang, X., Xie, L., Lu, S., Su, H., 2020a. Detection and diagnosis of oscillations in process control by fast adaptive chirp mode decomposition. Control Eng. Pract. 97, 104307. http://dx.doi.org/10.1016/j.conengprac.2020.104307, URL https://linkinghub.elsevier.com/retrieve/pii/S096706612030006X.

Chen, Q., Fei, X., Xie, L., Li, D., Wang, Q., 2020b. Causality analysis in process control based on denoising and periodicity-removing CCM. J. Intell. Manuf. Spec. Equip. 1 (1), 25–41. http://dx.doi.org/10.1108/JIMSE-06-2020-0003, URL https://www.emerald.com/insight/content/doi/10.1108/JIMSE-06-2020-0003/full/html.

Chen, Q., Lang, X., Xie, L., Su, H., 2019. Detecting oscillations via adaptive chirp mode decomposition. In: 2019 CAA Symposium on Fault Detection, Supervision and Safety for Technical Processes. SAFEPROCESS, IEEE, Xiamen, China, pp. 298–303. http://dx.doi.org/10.1109/SAFEPROCESS45799.2019.9213346, URL https://ieeexplore.ieee.org/document/9213346/.

CSB, n.d. U.S. Chemical Safety and Hazard Investigation Board | CSB. Retrieved 2023. URL https://www.csb.gov/.

Ding, S.X., 2014. Data-Driven Design of Fault Diagnosis and Fault-Tolerant Control Systems. In: Advances in Industrial Control, Springer London, London, http://dx.doi.org/10.1007/978-1-4471-6410-4, URL http://link.springer.com/10.1007/978-1-4471-6410-4.

Dragomiretskiy, K., Zosso, D., 2014. Variational mode decomposition. IEEE Trans. Signal Process. 62 (3), 531–544. http://dx.doi.org/10.1109/TSP.2013.2288675, URL http://ieeexplore.ieee.org/document/6655981/.

Frei, M.G., Osorio, I., 2007. Intrinsic time-scale decomposition: time–frequency–energy analysis and real-time filtering of non-stationary signals. Proc. R. Soc. A Math. Phys. Eng. Sci. 463 (2078), 321–342. http://dx.doi.org/10.1098/rspa.2006.1761, URL https://royalsocietypublishing.org/doi/10.1098/rspa.2006.1761.

Gilles, J., 2013. Empirical wavelet transform. IEEE Trans. Signal Process. 61 (16), 3999–4010. http://dx.doi.org/10.1109/TSP.2013.2265222, URL https://ieeexplore.ieee.org/document/6522142/.

Gilles, J., Heal, K., 2014. A parameterless scale-space approach to find meaningful modes in histograms — Application to image and spectrum segmentation. Int. J. Wavelets Multiresolut. Inform. Process. 12 (06), 1450044. http://dx.doi.org/10.1142/S0219691314500441, URL https://www.worldscientific.com/doi/abs/10.1142/S0219691314500441.

Guo, Z., Shen, J., Xie, L., Chen, X., Su, H., 2014a. Automatic detection of multiple oscillations by wavelet analysis. Comput. Electr. Eng. 40 (7), 2167–2177. http://dx.doi.org/10.1016/j.compeleceng.2014.03.007, URL https://linkinghub.elsevier.com/retrieve/pii/S0045790614000615.

Guo, Z., Xie, L., Ye, T., Horch, A., 2014b. Online detection of time-variant oscillations based on improved ITD. Control Eng. Pract. 32, 64–72. http://dx.doi.org/10.1016/j.conengprac.2014.07.002, URL https://linkinghub.elsevier.com/retrieve/pii/S0967066114001725.

Hardstone, R., Poil, S.-S., Schiavone, G., Jansen, R., Nikulin, V.V., Mansvelder, H.D., Linkenkaer-Hansen, K., 2012. Detrended fluctuation analysis: A scale-free view on neuronal oscillations. Front. Physiol. 3, http://dx.doi.org/10.3389/fphys.2012.00450, URL http://journal.frontiersin.org/article/10.3389/fphys.2012.00450/abstract.

Horch, A., 1999. A simple method for detection of stiction in control valves. Control Eng. Pract. 7 (10), 1221–1231. http://dx.doi.org/10.1016/S0967-0661(99)00100-8, URL https://linkinghub.elsevier.com/retrieve/pii/S0967066199001008.

HSE, n.d. HSE: Information about health and safety at work. Retrieved 2023. URL https://www.hse.gov.uk/.

Hu, Y., Li, F., Li, H., Liu, C., 2017. An enhanced empirical wavelet transform for noisy and non-stationary signal processing. Digit. Signal Process. 60, 220–229. http://dx.doi.org/10.1016/j.dsp.2016.09.012, URL https://linkinghub.elsevier.com/retrieve/pii/S1051200416301622.

Hurst, H.E., 1951. Long-term storage capacity of reservoirs. Trans. Am. Soc. Civ. Eng. 116 (1), 770–799. http://dx.doi.org/10.1061/TACEAT.0006518, URL http://ascelibrary.org/doi/10.1061/TACEAT.0006518.

Jelali, M., Huang, B. (Eds.), 2010. Detection and Diagnosis of Stiction in Control Loops. In: Advances in Industrial Control, Springer London, London, http://dx.doi.org/10.1007/978-1-84882-775-2, URL http://link.springer.com/10.1007/978-1-84882-775-2.

Jelali, M., Huang, B., 2021. Deteaction and diagnosis of stiction in control loops. URL https://sites.ualberta.ca/~bhuang/Stiction-Book.htm.

Kantz, H., Schreiber, T., 2003. Nonlinear Time Series Analysis, second ed. Cambridge University Press, http://dx.doi.org/10.1017/CBO9780511755798.

Lang, X., Xie, L., Sun, Y., Su, H., 2016. Automatic oscillation detection based on improved local mean decomposition. In: 2016 35th Chinese Control Conference (CCC). IEEE, Chengdu, pp. 6766–6771. http://dx.doi.org/10.1109/ChiCC.2016.7554423, URL https://ieeexplore.ieee.org/document/7554423/.

Lejay, A., Pigato, P., 2017. Statistical Estimation of the Oscillating Brownian Motion. http://dx.doi.org/10.48550/ARXIV.1701.02129, URL https://arxiv.org/abs/1701.02129. Publisher: arXiv Version Number: 1.

Li, X., Wang, J., Huang, B., Lu, S., 2010. The DCT-based oscillation detection method for a single time series. J. Process Control 20 (5), 609–617. http://dx.doi.org/10.1016/j.jprocont.2010.02.012, URL https://linkinghub.elsevier.com/retrieve/pii/S0959152410000600. Number: 5.

Matsuo, T., Tadakuma, I., Thornhill, N.F., 2004. Diagnosis of a unit-wide disturbance caused by saturation in a manipulated variable.

Miao, T., Seborg, D., 1999. Automatic detection of excessively oscillatory feedback control loops. In: Proceedings of the 1999 IEEE International Conference on Control Applications. Vol. 1. Cat. No.99CH36328, IEEE, Kohala Coast, HI, USA, pp. 359–364. http://dx.doi.org/10.1109/CCA.1999.806659, URL http://ieeexplore.ieee.org/document/806659/.

Naghoosi, E., Huang, B., 2014. Automatic detection and frequency estimation of oscillatory variables in the presence of multiple oscillations. Ind. Eng. Chem. Res. 53 (22), 9427–9438. http://dx.doi.org/10.1021/ie4037998, URL https://pubs.acs.org/doi/10.1021/ie4037998. Number: 22.

National Research Council, 1997. Digital Instrumentation and Control Systems in Nuclear Power Plants: Safety and Reliability Issues. National Academies Press, Washington, D.C., http://dx.doi.org/10.17226/5432, URL http://www.nap.edu/catalog/5432. Pages: 5432.

Peng, C.-K., Buldyrev, S.V., Havlin, S., Simons, M., Stanley, H.E., Goldberger, A.L., 1994. Mosaic organization of DNA nucleotides. Phys. Rev. E 49 (2), 1685–1689. http://dx.doi.org/10.1103/PhysRevE.49.1685, URL https://link.aps.org/doi/10.1103/PhysRevE.49.1685.

Peng, C.-K., Havlin, S., Stanley, H.E., Goldberger, A.L., 1995. Quantification of scaling exponents and crossover phenomena in nonstationary heartbeat time series. Chaos 5 (1), 82–87. http://dx.doi.org/10.1063/1.166141, URL http://aip.scitation.org/doi/10.1063/1.166141.

Riley, M.A., Van Orden, G.C., Foundation (U.S.), N.S., 2005. In: Michael A. Riley, Guy C. Van Orden (Eds.), Tutorials in Contemporary Nonlinear Methods for the Behavioral Sciences [Electronic Resource]. National Science Foundation, Arlington, VA, Type: Book.

Srinivasan, B., Rengaswamy, R., 2012. Automatic oscillation detection and characterization in closed-loop systems. Control Eng. Pract. 20 (8), 733–746. http://dx.doi.org/10.1016/j.conengprac.2012.02.008, URL https://linkinghub.elsevier.com/retrieve/pii/S096706611200055X.

Srinivasan, R., Rengaswamy, R., Miller, R., 2007. A modified empirical mode decomposition (EMD) process for oscillation characterization in control loops. Control Eng. Pract. 15 (9), 1135–1148. http://dx.doi.org/10.1016/j.conengprac.2007.01.014, URL https://linkinghub.elsevier.com/retrieve/pii/S0967066107000263. Number: 9.

Thornhill, N., Huang, B., Zhang, H., 2003. Detection of multiple oscillations in control loops. J. Process Control 13 (1), 91–100. http://dx.doi.org/10.1016/S0959-1524(02)00007-0, URL https://linkinghub.elsevier.com/retrieve/pii/S0959152402000070. Number: 1.

Turcotte, D.L., 1997. Fractals and Chaos in Geology and Geophysics, second ed. Cambridge University Press, http://dx.doi.org/10.1017/CBO9781139174695, URL https://www.cambridge.org/core/product/identifier/9781139174695/type/book.

Wang, J., Huang, B., Lu, S., 2013. Improved DCT-based method for online detection of oscillations in univariate time series. Control Eng. Pract. 21 (5), 622–630. http://dx.doi.org/10.1016/j.conengprac.2012.12.007, URL https://linkinghub.elsevier.com/retrieve/pii/S0967066112002614. Number: 5.

Wardana, A.N.I., 2015. A method for detecting the oscillation in control loops based on variational mode decomposition. In: 2015 International Conference on Computer, Control, Informatics and Its Applications. IC3INA, IEEE, Bandung, Indonesia, pp. 181–186. http://dx.doi.org/10.1109/IC3INA.2015.7377769, URL http://ieeexplore.ieee.org/document/7377769/.

Wardana, A.N.I., 2016. A comparative study of EMD, EWT and VMD for detecting the oscillation in control loop. In: 2016 International Seminar on Application for Technology of Information and Communication. ISemantic, IEEE, Semarang, Indonesia, pp. 58–63. http://dx.doi.org/10.1109/ISEMANTIC.2016.7873810, URL http://ieeexplore.ieee.org/document/7873810/.

Wu, Z., Huang, N.E., 2009. Ensemble empirical mode decomposition: A noise-assisted data analysis method. Adv. Adapt. Data Anal. 01 (01), 1–41. http://dx.doi.org/10.1142/S1793536909000047, URL https://www.worldscientific.com/doi/abs/10.1142/S1793536909000047.

Xie, L., Lang, X., Horch, A., Yang, Y., 2016. Online oscillation detection in the presence of signal intermittency. Control Eng. Pract. 55, 91–100. http://dx.doi.org/10.1016/j.conengprac.2016.06.020, URL https://linkinghub.elsevier.com/retrieve/pii/S0967066116301472.

Zheng, J., Pan, H., Yang, S., Cheng, J., 2017. Adaptive parameterless empirical wavelet transform based time-frequency analysis method and its application to rotor rubbing fault diagnosis. Signal Process. 130, 305–314. http://dx.doi.org/10.1016/j.sigpro.2016.07.023, URL https://linkinghub.elsevier.com/retrieve/pii/S0165168416301748.

Zhivomirov, H., 2018. A method for colored noise generation. Romanian J. Acoust. Vib. 15, 14–19.

Zhuang, C., Liao, P., 2020. An improved empirical wavelet transform for noisy and non-stationary signal processing. IEEE Access 8, 24484–24494. http://dx.doi.org/10.1109/ACCESS.2020.2968851, URL https://ieeexplore.ieee.org/document/8967110/.